Key Points:
- The high-precision densities and porosities of 214 fragments from 163 different ordinary chondrites (OCs) including falls, non-Antarctic finds, and Antarctic finds were measured and calculated; the pore morphology of some selected OCs were investigated
- Weak shock (<S2) may increase the porosity of a meteorite by generating tiny cracks to link some isolated pores; shock degree ≥S3 will compact the material and significantly reduce the porosities of OCs
- The high-precision grain density and porosity data of OCs can be used to infer in inner structure of an OC analogous asteroid

Supporting Information:
- Supporting Information S1

Correspondence to:
S. J. Li,
ldlshijie@126.com

The Density, Porosity, and Pore Morphology of Fall and Find Ordinary Chondrites

S. J. Li[1,2] iD, **S. J. Wang[3], B. K. Miao[4], Y. Li[1,2], X. Y. Li[1,2], X. J. Zeng[1], and Z. P. Xia[4]**

[1]Center for Lunar and Planetary Sciences, Institute of Geochemistry, Chinese Academy of Sciences, Guiyang, China, [2]Center for Excellence in Comparative Planetology, Chinese Academy of Sciences, Hefei, China, [3]State Key Laboratory of Environmental Geochemistry, Institute of Geochemistry, Chinese Academy of Sciences, Guiyang, China, [4]Department of Resources and Environmental Engineering, Guilin University of Technology, Guilin, China

Abstract Density, porosity, and pore morphology constitute the basic physical properties of meteorites. These properties of 214 fragments from 163 different ordinary chondrites (OCs), including falls, non-Antarctic finds, and Antarctic finds, were measured, calculated, and investigated. Of all the measured OCs data, densities, and porosities of 37 OC falls (14 H, 17 L, and 6 LL), 31 non-Antarctic finds (9 H and 22 L), and 95 Antarctic finds (24 H and 73 L) are reported for the first time. The individual masses of all the meteorite fragments measured in this study ranged between 0.8953 and 7.7133 g, and these masses were too low to be measured by the Archimedean glass bead method. Our study indicated that the grain density and porosity of find OCs are significantly reduced by terrestrial weathering. As a result, such OCs are not suitable for their physical propertie study. Shock degree ≤S2 slightly increases the measurable porosities of the meteorites by generating a certain amount of tiny cracks in the silicates to connect some isolated pores with the measurable pores. Shock degree over S2 significantly reduces the porosities of meteorites by compacting or even melting the material. Weathering reduced the porosities via space filling of weathering products. Shock load over S2 reduced the porosities of the meteorites by minerals compressing or melting. Moreover, the shock load over S2 also converted intergrain irregular pores into intragrain cracks. Thermal metamorphism mainly changed the pore morphology (size) by pore merging during mineral recrystallization. The pore morphology also plays a significant role in controlling the friability of OCs.

Plain Language Summary This study aimed to obtain high-precision density and porosity data for ordinary chondrites (OCs) and to understand the major influences on these properties. The grain densities, bulk densities, and porosities of 214 small (0.8953–7.7133 g) OC fragments of falls, non-Antarctic finds, and Antarctic finds were measured using the high-precision Pycnometer-balloon vacuum packing method. The Grove Mountain OCs from Antarctica and falls in China have seldom studied in previous works. Moreover, the pore morphologies of the OCs were systematically observed. The results indicated that the grain densities and porosities of non-Antarctic finds and Antarctic finds were significantly altered by terrestrial weathering. Shock strength ≤S2 increases measurable porosities by generating intragrain cracks and connecting some isolated pores. However, shock intensity over S2 reduces the porosities of meteorites by minerals compressing or melting. Thermal metamorphism changes the pore morphology by pore merging during mineral recrystallization. Our high-precision porosity and density data can be used not only to evaluate the homogeneity of a meteorite shower samples but also to understand the structures of S-type asteroids.

1. Introduction

Density and porosity are the basic physical properties of meteorites, and they reflect the ambient circumstances of meteorite formation and evolution. Previous investigations suggested that some asteroids (e.g., Deimos, 45 Eugenia, 433 Eros, and 16 Psyche) could have numerous porous areas, or macrocracks, based on comparisons of the measured densities and porosities of meteorites to the flyby or ground-based data (Britt et al., 2002; Consolmagno et al., 2008; Flynn et al., 1999; Shepard et al., 2017; Wilkison et al., 2003; Wilkison & Robinson, 2000). In particular, the rubble-pile structure of the asteroid Itokawa is also deduced from the comparison of its bulk density to that of LL ordinary chondrites (OCs; Fujiwara et al., 2006). Some scientists used the measured density (or porosity) of meteorites or lunar rocks to evaluate their remote sensing interpreted data (e.g., Huang & Wieczorek, 2012, and the references therein). In addition, porosity is an

important parameter that can affect other physical properties (e.g., thermal conductivity, seismic velocity, actual cosmic ray shading depth, and electrical conductivity; Britt et al., 2002).

To determine the values and factors that control or influence the densities and porosities of meteorites, a number of studies have been performed, and various measuring methods have been utilized in the past 60 years (Alexeyeva, 1958; Corrigan et al., 1997; Consolmagno et al., 1998, 2008; Consolmagno & Britt, 1998; Flynn et al., 1999; Britt & Consolmagno, 2000, 2003; Wilkison et al., 2003; Macke, Consolmagno, et al., 2010, Macke, Britt, & Consolmagno, 2011, Macke, Consolmagno, & Britt, 2011; Kiefer et al., 2012; Kohout et al., 2014). To date, eight kinds of methods have been used to determine the bulk volume (or porosity) of a meteorite: (1) determining point count using the backscattered electron (BSE) images (e.g., Corrigan et al., 1997; Strait & Consolmagno, 2002, 2005); (2) immersing the meteorite in a certain liquid (e.g., Keil, 1962; Kukkonen & Pesonen, 1983; Pesonen et al., 1993; Terho et al., 1993); (3) processing the meteorite into a regular geometry (e.g., Yomogida & Matsui, 1981); (4) wrapping the meteorite with a known volume clay and processing the clay surface into a regular geometry (e.g., Matsui et al., 1980; Yomogida & Matsui, 1983); (5) performing the Archimedean bead method (e.g., Britt & Consolmagno, 2003; Consolmagno & Britt, 1998; Coulson et al., 2007; Kiefer et al., 2012; Macke, Britt, & Consolmagno, 2010; Macke, Britt, & Consolmagno, 2011; Macke, Consolmagno, et al., 2010; Macke, Consolmagno, & Britt, 2011; Sasso et al., 2009; Wilkison et al., 2003); (6) performing 3-D laser imaging (Herd et al., 2003; McCausland et al., 2011; Smith et al., 2006); (7) performing X-ray microtomography (Friedrich et al., 2008; McCausland et al., 2010; Wittmann et al., 2011); and (8) performing the Pycnometer-balloon vacuum packing method (Li et al., 2012). Considering the variety of defects associated with these methods (e.g., destructive, contaminating, and low precision), the first four methods have been eliminated by most scientists. The Archimedean bead method, the preferred method to measure the bulk volume of meteorites, has many advantages, such as being nondestructive, noncontaminating, economical, and easy to perform (e.g., Britt & Consolmagno, 2003; Consolmagno & Britt, 1998; Coulson et al., 2007; Kiefer et al., 2012; Kohout et al., 2014; Macke, Britt, & Consolmagno, 2010; Macke, Britt, & Consolmagno, 2011; Macke, Consolmagno, et al., 2010; Macke, Consolmagno, & Britt, 2011; Sasso et al., 2009; Wilkison et al., 2003). However, the precision and accuracy of the Archimedean bead method dramatically decrease with decreasing meteorite volume when applied to a sample smaller than 15 cm^3 (Macke, Britt, & Consolmagno, 2010). The 3-D laser imaging and X-ray microtomography methods are suitable for determining the bulk volumes of meteorites with a small-sized samples of ~0.5 cm^3 (McCausland et al., 2010, 2011), while many factors (e.g., expensive and time-consuming) make these two methods difficult to be widely used (Friedrich et al., 2008; Herd et al., 2003; McCausland et al., 2010, 2011; Smith et al., 2006; Wittmann et al., 2011). Pycnometer-balloon vacuum packing method can be considered simple, nondestructive, and noncontaminating, and it can obtain reliable results even for small-sized samples (~0.5 cm^3) (Li et al., 2012).

To date, many studies relevant to the densities and porosities of OCs have been performed (Matsui et al., 1980; Yomogida & Matsui, 1981; Yomogida & Matsui, 1983; Terho et al., 1993; Pesonen et al., 1993; Corrigan et al., 1997; Consolmagno et al., 1998; Consolmagno & Britt, 1998; Wilkison & Robinson, 2000; Wilkison et al., 2003; Przylibski et al., 2003; Smith et al., 2006; Consolmagno et al., 2006; Beech et al., 2009; McCausland et al., 2011; Kohout et al., 2011; Friedrich et al., 2013; Friedrich & Rivers, 2013; Kohout et al., 2014). These data have been used to discuss the inner structures of rocky asteroids (Britt et al., 2002; Consolmagno et al., 2008; Flynn et al., 1999; Wilkison & Robinson, 2000). Moreover, the factors (e.g., terrestrial weathering, thermal metamorphism, and shock) that might affect the densities and porosities have been investigated (e.g., Consolmagno et al., 1998; Macke, 2010). However, the following aspects about the densities and porosities of OCs are still not clear: (1) the occurrences of pores in different petrologic types and different shock stages; (2) the influences on densities and porosities of OCs under different collecting environments (e.g., hot and cold desert); and (3) the minor differences between samples, which could be obtained from more high accuracy and high precision data of densities and porosities of OCs (particularly for the small-sized meteorite fragments).

In this study, the densities and porosities of 163 OCs (H, L, and LL groups) were measured and investigated. All of the samples measured in this work were too small in size to be tested with the Archimedean glass bead method. Many Chinese fall OCs and Antarctic Grove Mountain find OCs have not yet been measured in previous studies. The purpose of our study is to discuss (1) the densities, porosities, and pore morphologies of the studied meteorites and how these properties are affected by terrestrial weathering, thermal

metamorphism, and shock events and (2) the porosities of some S-type asteroids and the inner structures of S-type asteroids.

2. Samples and Methods

The meteorites studied included 37 OC falls (the densities and porosities of five samples were already reported in Li et al., 2012, and Li, et al., 2017), 95 Antarctic OCs, and 31 non-Antarctic find OCs with masses between 0.8953 and 7.7133 g. The polished sections of some representative OCs were also investigated.

2.1. Measurements of Grain Density, Bulk Density, and Porosity

The grain densities, bulk densities, and porosities of OCs were measured using a Micro-Ultrapyc 1200e ideal gas pycnometer according to the method described in Li et al. (2012). Briefly, the method works according to the following steps: (1) weighing the analyzed meteorite mass (M_m) with a balance; (2) measuring the grain density (ρ_g) and grain volume (V_g) of the meteorite with the pycnometer; (3) vacuum-packing the meteorite with a thin-wall balloon, and then measuring the volume ($V_t=V_b+V_{bl}$; bulk volume of the meteorite plus the volume of the balloon) of the packed meteorite and the balloon with the pycnometer; (4) measuring the volume (V_{bl}) of the balloon, after removing the meteorite, with the pycnometer; and (5) calculating the bulk volume ($V_b= V_t-V_{bl}$), bulk density ($\rho_b=M_m/V_b$), and porosity [$P=(V_b-V_g)/V_b*100\%$] of the measured meteorite.

In this paper, 214 fragments from 163 different OCs were measured. Among these OC fragments, 58 are falls, 44 are non-Antarctic finds, and 112 are Antarctic finds (81 only were measured for grain density). There were no visible cracks in these fragments. The measuring gas was high purity N_2 (purity ≥99.999%, H_2O+O_2≤5 ppm, H_2≤1 ppm, and ΣC≤ 3ppm), and the gas pressure of the measurement was ~ 0.135 MPa (19.5 psi).

2.2. The Investigation of Pores

Some OCs were selected, and their polished sections were made to investigate how the pore morphologies responded to thermal metamorphism, shock effects, and weathering processes. This work was carried out on a SM-6460LV scanning electron microscope (SEM) and a Scios-FIB field emission SEM at the Institute of Geochemistry, Chinese Academy of Sciences. High-resolution BSE images were also obtained under the two SEMs previously mentioned.

3. Results

We divided these OCs (214 fragments from 163 different meteorites) into three groups, for example, falls, non-Antarctic finds, and Antarctic meteorites. These fragments were composed of 58 fragments from 37 different falls (14 H OCs, 17 L OCs, and 6 LL OCs), 44 fragments from 31 different non-Antarctic finds (9 H OCs and 22 L OCs), and 112 fragments from 95 different Antarctic finds (24 H OCs and 73 L OCs). Among the Antarctic OCs, only 64 out of 95 only had the grain densities been measured. The basic information, such as name, mass, and petrographic type of the studied meteorites, can be seen in Tables 1–3.

3.1. Density and Porosity

The measured grain densities, bulk densities, and porosities are shown in Table 1–3 and Figure 1. For OC falls, the grain densities of 14 H chondrites vary between 3.657±0.003 and 3.980±0.006 g/cm³, with an average value of 3.776±0.062 g/cm³ (or 3.793±0.047 g/cm³ if the weathered [W1] Laochenzhen and the Gao-Guenie are removed). In particular, the H5 chondrite Huaxi has the highest grain density of 3.890±0.006 g/cm³, averaged from four fragments. The grain densities of the Laochenzhen and the Gao-Guenie are 3.657±0.003 and 3.689±0.005 g/cm³, respectively, which are relatively lower than those of other H falls in this study. These two fragments are clearly weathered to some extent, which might be the reason for their low grain densities. The bulk densities of these 14 H chondrites range from 3.040±0.005 to 3.624±0.008 g/cm³, with an average value of 3.404±0.163 g/cm³ (3.371±0.151 g/cm³ without the Laochenzhen and the Gao-Guenie). The porosities of these 14 H OCs range from 0.91±0.23% to 17.61±0.23%, with an average of 9.78 ±5.44% (11.09±4.66% without the Laochenzhen and the Gao-Guenie). Similar to grain densities, the porosities of the Laochenzhen and the Gao-Guenie are 0.91±0.23% and 2.93±0.26%, respectively, which are much lower when compared with those values of other H falls studied. Again, the low porosities of these two

Table 1
Mass, Volume, Density, and Porosity Values of Measured Fall Ordinary Chondrites

Sample	Mass (g)	Grain volume (cm^3)	1sd	Bulk volume (cm^3)	1sd	Grain density (g/cm^3)	1sd	Bulk density (g/cm^3)	1sd	Porosity (%)	1sd	Class	Shock stage	Weathering degree
Anlong-1	1.8373	0.497	0.001	0.604	0.001	3.699	0.010	3.040	0.005	17.81	0.27			
Anlong-2	4.5599	1.201	0.000	1.422	0.001	3.797	0.001	3.208	0.002	15.52	0.06			
Anlong ave.						3.768	0.004	3.158	0.003	16.20	0.12	H5	S2-3 (b-c, Wang, 1993)	W0
Chergach	5.6950	1.515	0.001	1.627	0.002	3.760	0.003	3.501	0.004	6.87	0.13	H5	S3-4 (MB, 94)[a]	W0
Enshi	3.1284	0.830	0.001	0.881	0.003	3.771	0.004	3.553	0.013	5.80	0.36	H5	S4 (d, Wang, 1993)[a]	W0
Gao-Guenie[b]	3.5107	0.952	0.001	0.980	0.002	3.689	0.005	3.581	0.008	2.93	0.26	H5	S3[a]	W1
Gao-Guenie (Beech et al., 2009)						3.53	0.08	3.46	0.07	2.46	1.39	H5		
Gao-Guenie (McCausland et al., 2011)	4.35							3.65	0.05			H5		
Huaxi-1[c]	2.2888	0.598	0.001	0.726	0.001	3.827	0.005	3.152	0.006	17.63	0.20			
Huaxi-2[c]	3.8277	0.961	0.001	1.164	0.002	3.981	0.004	3.288	0.006	17.43	0.18			
Huaxi-3[c]	2.8387	0.728	0.002	0.871	0.003	3.902	0.010	3.258	0.010	16.50	0.34			
Huaxi-4[c]	3.2644	0.854	0.001	1.051	0.002	3.822	0.006	3.107	0.006	18.71	0.21			
HX-ave						3.890	0.006	3.205	0.007	17.61	0.23	H5	S2 (Li et al., 2017)	W0
Jilin-1[b]	3.4483	0.903	0.001	0.999	0.003	3.817	0.003	3.451	0.010	9.59	0.26			
Jilin-2[b]	4.2298	1.106	0.001	1.204	0.002	3.824	0.003	3.515	0.007	8.08	0.20			
Jilin-3[b]	3.7014	0.972	0.001	1.097	0.002	3.808	0.004	3.375	0.007	11.37	0.21			
Jilin-4[b]	3.3059	0.881	0.001	0.957	0.003	3.751	0.003	3.456	0.010	7.86	0.28			
Jilin-5[b]	4.8352	1.284	0.000	1.404	0.004	3.765	0.001	3.444	0.010	8.51	0.28			
Jilin-6[b]	4.0572	1.073	0.011	1.176	0.002	3.780	0.038	3.449	0.005	8.76	0.95			
jilin-7	4.8247	1.288	0.001	1.399	0.001	3.746	0.003	3.449	0.002	7.91	0.08			
Jilin-8	2.8397	0.743	0.001	0.785	0.001	3.824	0.004	3.619	0.003	5.37	0.10			
Jilin-9	2.3708	0.621	0.000	0.668	0.001	3.816	0.002	3.551	0.003	6.94	0.09			
Jilin-10	2.9087	0.764	0.001	0.837	0.002	3.807	0.005	3.476	0.008	8.68	0.22			
Jilin-11	1.9593	0.526	0.000	0.572	0.002	3.727	0.001	3.424	0.012	8.14	0.32			
Jilin-12	2.2062	0.568	0.001	0.608	0.001	3.882	0.007	3.630	0.006	6.50	0.21			
JL-ave						3.792	0.006	3.476	0.007	8.32	0.24	H5	S3 (Stöffler et al., 1991)[a]	W0
Jilin (Macke, 2010)	33.56					3.70	0.02	3.49	0.06	5.7	1.8	H5		
Jilin (Beech et al., 2009)	62.35					3.78	0.04	3.41	0.03	9.8	0.01	H5		
Jilin (Kohout et al., 2008)	73.4					3.925		3.398		13		H5		
Juancheng	1.9761	0.526	0.001	0.562	0.002	3.756	0.008	3.514	0.013	6.44	0.40	H5	S3[a]	W0
Juancheng (Macke, 2010)	43.54					3.63	0.01	3.61	0.04	0.7	1.1	H5		
Juancheng (Kohout et al., 2008)	17.93					3.815		3.898				H5		
Laochenzhen	2.4229	0.663	0.001	0.669	0.001	3.657	0.003	3.624	0.008	0.91	0.23	H5	S4 (b-c, Wang, 1993)[a]	W1
Shuangyang	2.9350	0.772	0.000	0.894	0.002	3.803	0.002	3.282	0.006	13.71	0.16	H5	S2-3 (b-c, Wang, 1993)	W0

Table 1 (continued)

Sample	Mass (g)	Grain volume (cm^3)	1sd	Bulk volume (cm^3)	1sd	Grain density (g/cm^3)	1sd	Bulk density (g/cm^3)	1sd	Porosity (%)	1sd	Class	Shock stage	Weathering degree
Tamdakht	1.3937	0.371	0.002	0.387	0.002	3.754	0.037	3.600	0.015	4.08	0.72	H5	S3 (MB, 95)	W0
Zaoyang[b]	3.1769	0.826	0.013	1.002	0.002	3.847	0.016	3.172	0.007	17.54	1.33			
Zaoyang-2	3.2175	0.859	0.001	0.987	0.002	3.746	0.002	3.261	0.007	12.95	0.20			
Zaoyang ave.						3.796	0.031	3.216	0.007	15.27	0.71	H5	S2 (b, Wang & Rubin, 1987)	W0
Zaoyang (Macke, 2010)	28.07					3.72	0.02	3.09	0.03	17.0	1.0	H5		
Lunan	4.3520	1.123	0.001	1.316	0.001	3.877	0.002	3.306	0.003	14.73	0.09	H6	S2-3 (b-c, Wang, 1993)	W0
Wuan-1	4.9845	1.303	0.003	1.514	0.003	3.826	0.008	3.292	0.007	13.94	0.25			
Wuan-2	5.1355	1.355	0.003	1.570	0.002	3.791	0.008	3.270	0.004	13.73	0.21			
Wuan ave.						3.808	0.008	3.281	0.006	13.83	0.23	H6	S2 (b, Wang, 1993)	W0
Xingyang	0.8953	0.239	0.002	0.267	0.002	3.743	0.030	3.358	0.024	10.28	0.96	H6	S1-2 (a-b, Wang, 1993)	W0
H ave.						3.776	0.062	3.404	0.163	9.78	5.44			
Heyetang	2.4946	0.688	0.003	0.702	0.002	3.625	0.013	3.555	0.012	1.92	0.49	L3	S1(Shen et al., 2013)	W1
Xinglongquan	2.1258	0.587	0.002	0.653	0.002	3.624	0.012	3.258	0.010	10.100	0.39	L3	S1(MB, 104)	W0
Zhaodong-1[b]	5.0099	1.388	0.001	1.476	0.003	3.610	0.002	3.394	0.007	5.975	0.20			
Zhaodong-2	4.1209	1.149	0.002	1.221	0.001	3.588	0.005	3.376	0.002	5.906	0.16			
Zhaodong ave.						3.600	0.003	3.386	0.005	5.944	0.16	L4	S3 (c, Wang, 1993)	W0
Zhaodong (Macke, 2010)	66.32					3.60	0.01	3.46	0.03	3.9	-0.9	L4		
Mount Tazerzait	0.9982	0.295	0.001	0.313	0.002	3.384	0.006	3.185	0.017	5.871	0.53	L5	S1 (Friedrich et al., 2014)	W0
Mount Tazerzait (Kohout et al., 2008)	12.9					4.031		3.000		26		L5		
Taonan	1.6243	0.445	0.001	0.524	0.001	3.653	0.005	3.102	0.007	15.069	0.22	L5	S2 (b, Wang, 1993)	W0
Xining	2.7826	0.768	0.001	0.868	0.004	3.622	0.005	3.204	0.014	11.527	0.40	L5	S3 (MB, 102)	W0
Mocs	3.6652	1.023	0.000	1.122	0.002	3.584	0.001	3.266	0.005	8.884	0.15	L5-6	S3-5 (Macke, 2010)[a]	W0
Mocs (19; Macke, 2010)[d]						3.63		3.26		10.3		L5-6		
						3.44	0.02	3.14	0.03	9	1.1	L5-6		

Table 1 *(continued)*

Sample	Mass (g)	Grain volume (cm^3)	1sd	Bulk volume (cm^3)	1sd	Grain density (g/cm^3)	1sd	Bulk density (g/cm^3)	1sd	Porosity (%)	1sd	Class	Shock stage	Weathering degree
Mocs (6; Consolmagno & Britt, 1998)[d]														
Mocs (8; Consolmagno et al., 2006)[d]						3.67	0.02	3.33	0.04	7.68-10.38		L5-6		
Mocs (Kohout et al., 2008)	57.2					3.667		3.467		5		L5-6		
Mocs (Kohout et al., 2008)	36.l5					3.65		3.288		10		L5-6		
Mocs (Smith et al., 2006)	29.87							3.30				L5-6		
Mocs (Smith et al., 2006)	151.0							3.35				L5-6		
Mocs (Wilkison & Robinson, 2000)	840.40					3.49	0.08	3.25	0.03	6.9	2.3	L5-6		
Mocs (Wilkison & Robinson, 2000)	39.51							3.29	0.02			L5-6		
Battle Mountain	2.8123	0.786	0.002	0.845	0.002	3.577	0.011	3.327	0.007	7.003	0.30	L6	S4 (MB, 101)[a]	W0
Berduc	2.3308	0.661	0.001	0.722	0.003	3.526	0.011	3.228	0.014	8.435	0.41	L6	S4 (MB, 96)[a]	W0
Boumdeid (2011)	1.6908	0.463	0.001	0.531	0.002	3.650	0.009	3.182	0.011	12.818	0.37	L6	S2 (MB, 95)	W0
Bruderheim	2.7478	0.763	0.001	0.838	0.002	3.604	0.004	3.279	0.009	8.999	0.27	L6	S3	W0
Colby (Wisconsin)	1.6172	0.435	0.001	0.477	0.002	3.716	0.005	3.393	0.014	8.687	0.39	L6	S3(Macke, 2010)	W0
Colby (Wisconsin; Macke, 2010)	21.819					3.56	0.02	3.38	0.04	5.0	1.3			
Colby (Wisconsin; Wilkison & Robinson, 2000)	34.32							3.48	0.03					
Guangnan	2.9062	0.834	0.000	0.862	0.002	3.484	0.000	3.373	0.006	3.180	0.19	L6	S2-3 (b-c, Wang, 1993)	W2 (Wang & Rubin, 1987)
Holbrook-1_1	3.403	0.952	0.001	1.091	0.001	3.576	0.002	3.118	0.003	12.809	0.11			
Holbrook-1_1	3.4027	0.956	0.000	1.083	0.001	3.559	0.001	3.142	0.004	11.726	0.11			
Holbrook-1 ave.	3.40285	0.954	0.000	1.087	0.001	3.568	0.002	3.130	0.004	12.267	0.11			
Holbrook-2	3.8117	1.066	0.001	1.210	0.001	3.576	0.002	3.149	0.004	11.939	0.11			
Holbrook ave.						3.572	0.002	3.140	0.004	12.10	0.11	L6	S2	W0
Holbrook (36; Macke, 2010)[d]						3.55		3.18		10.4		L6		
Holbrook (22; Consolmagno et al., 2006)[d]						3.67	0.04	3.41	0.09	0.26-11.07		L6		
Holbrook (Kohout et al., 2008)	15.77					3.755		3.092		18		L6		
	57.30							3.36	0.03			L6		

Table 1 *(continued)*

Sample	Mass (g)	Grain volume (cm^3)	1sd	Bulk volume (cm^3)	1sd	Grain density (g/cm^3)	1sd	Bulk density (g/cm^3)	1sd	Porosity (%)	1sd	Class	Shock stage	Weathering degree
Holbrook (Wilkison & Robinson, 2000)														
Jartai	3.0591	0.855	0.001	0.901	0.002	3.578	0.002	3.395	0.008	5.094	0.23	L6	S3 (c, Wang, 1993)	W0
Suizhou	2.9534	0.829	0.002	0.859	0.002	3.562	0.008	3.437	0.008	3.537	0.31	L6	S4 (Xie et al., 2001)[a]	W0
Suizhou (Macke, 2010)	40.02					3.56	0.02	3.22	0.03	9.5	1.0			
Xi Ujimgin	1.2064	0.338	0.002	0.355	0.001	3.566	0.016	3.403	0.013	4.570	0.56	L/ LL6-an	S3 (c, Wang, 1993)	W0
L ave.						3.584	0.074	3.301	0.121	7.867	3.70			
Bo Xian	3.3309	0.953	0.002	1.077	0.002	3.496	0.007	3.092	0.006	11.565	0.24	LL3	S2 (b, Wang, 1993)	W0
Vicência	2.0099	0.569	0.000	0.622	0.002	3.533	0.002	3.229	0.009	8.612	0.26	LL3	S1(MB, 103)	
Chelyabinsk-1	1.7056	0.482	0.000	0.518	0.002	3.541	0.003	3.293	0.010	7.008	0.28			
Chelyabinsk-2	3.1384	0.890	0.000	0.959	0.001	3.528	0.002	3.272	0.002	7.266	0.07			
Chelyabinsk ave.						3.532	0.002	3.279	0.005	7.175	0.14	LL5	S4 (Xu et al., 2016)[a]	W0
Kheneg Ljouâd	2.4975	0.711	0.000	0.789	0.001	3.511	0.001	3.167	0.005	9.802	0.15	LL5/6	S3 (MB, 106)[a]	W0
Dongtai-1	4.6263	1.306	0.001	1.558	0.001	3.543	0.002	2.970	0.002	16.161	0.09			
Dongtai-2	1.5648	0.443	0.001	0.524	0.001	3.535	0.004	2.989	0.008	15.435	0.25			
Dongtai-ave.						3.541	0.003	2.975	0.004	15.978	0.13	LL6	S2 (b, Wang, 1993)	W0
Kilabo_1	3.6126	1.038	0.001	1.150	0.002	3.479	0.002	3.141	0.004	9.721	0.14			
Kilabo_2	3.6126	1.039	0.001	1.150	0.002	3.478	0.004	3.141	0.004	9.686	0.17			
Kilabo ave.	3.6126	1.039	0.001	1.150	0.002	3.479	0.003	3.141	0.004	9.704	0.15	LL6	S3 (MB,87)	W0
LL ave						3.515	0.025	3.147	0.107	10.47	3.06			

Note. MB = Meteoritical Bulletin Database.
[a]Meteorite with shock veins or shock pocket. Shock degree in Wang (1993) is according to the criteria in Dodd and Jarosewich (1979). [b]The result of the meteorite fragment was reported in Li et al. (2012). [c]The result was reported in Li et al. (2017). [d]The number of meteorite fragments measured in literature.

meteorites should be related to weathering. For the Gao-Guenie, the shock process also accounts for the relatively lower porosity, which will be described in later. The grain densities of the 17 L OCs vary from 3.384 ± 0.006 to 3.716 ± 0.005 g/cm^3, with an average value of 3.584 ± 0.074 g/cm^3 (3.588 ± 0.073 g/cm^3 without the weathered Guangnan and the Heyetang). The bulk densities of these OCs are between 3.102 ± 0.007 and 3.555 ± 0.012 g/cm^3 with an average value of 3.301 ± 0.121 g/cm^3 (3.279 ± 0.106 g/cm^3 without the weathered Guangnan and the Heyetang). The porosities of the 17 L OCs are in the range of 1.92 ± 0.49 to $15.07\pm0.22\%$, with an average value of $7.87\pm3.70\%$ ($8.58\pm3.31\%$ without the Guangnan and the Heyetang). The Heyetang is an L fall with a very low porosity of $1.92\pm0.49\%$, which is likely due to the weathering degree of W1. The porosity of the Guangnan is $3.18\pm0.19\%$, and the meteorite was reported with a weathering degree of W2 (Wang & Rubin, 1987). For the six LL OCs, the grain densities are between 3.479 ± 0.003 and 3.541 ± 0.003 g/cm^3, with an average of 3.515 ± 0.025 g/cm^3. The bulk grain densities vary from 2.975 ± 0.004 to 3.293 ± 0.010 g/cm^3, with an average of 3.147 ± 0.107 g/cm^3. The porosities of the six LL OCs are in the range of $7.18\pm0.14\%$ to $15.98\pm0.13\%$, and the average value is $10.47\pm3.06\%$.

Table 2
Mass, Volume, Density, and Porosity Values of Measured Non-Antarctic Find Ordinary Chondrites

Sample	Mass (g)	Grain volume (cm³)	1sd	Bulk volume (cm³)	1sd	Grain density (g/cm³)	1sd	Bulk density (g/cm³)	1sd	Porosity (%)	1sd	Class	Shock stage	Weathering degree
Tulia (a)	1.8675	0.540	0.000	0.561	0.003	3.460	0.002	3.330	0.017	3.74	0.50	H3-4	S2	W1
NWA 4656	1.9825	0.549	0.001	0.624	0.002	3.614	0.008	3.180	0.009	12.01	0.32	H4	S2	W2
NWA 5778	1.7275	0.527	0.001	0.544	0.002	3.277	0.007	3.174	0.011	3.14	0.39	H4		
Travis County (b)	2.7649	0.831	0.001	0.850	0.002	3.326	0.005	3.252	0.007	2.22	0.25	H4	S4	
Hami 003	4.3156	1.226	0.001	1.232	0.001	3.521	0.003	3.504	0.003	0.47	0.11	H5	S2	W1
Hami 005	5.0948	1.476	0.001	1.493	0.007	3.452	0.001	3.413	0.016	1.12	0.47	H5	S3	W3
Kumtag-1	3.9208	1.073	0.001	1.079	0.002	3.655	0.004	3.635	0.008	0.56	0.23			
Kumtag-2	4.0848	1.136	0.000	1.140	0.002	3.595	0.001	3.585	0.007	0.28	0.21			
Kumtag-3	2.5674	0.709	0.000	0.723	0.002	3.622	0.002	3.551	0.009	1.96	0.25			
Kumtag-4	3.2497	0.931	0.000	0.939	0.001	3.491	0.002	3.462	0.004	0.82	0.12			
Kumtag-5_1	1.7933	0.485	0.001	0.497	0.002	3.697	0.005	3.611	0.015	2.32	0.43			
Kumtag-5_2	1.7933	0.490	0.001	0.501	0.001	3.663	0.004	3.578	0.004	2.33	0.14			
Kumtag-5 ave.	1.7933	0.487	0.001	0.499	0.001	3.680	0.004	3.595	0.010	2.33	0.29			
Kumtag-6	1.9524	0.551	0.001	0.557	0.001	3.541	0.005	3.507	0.006	0.95	0.19			
Kumtag-7	2.9210	0.810	0.001	0.825	0.001	3.606	0.003	3.540	0.005	1.84	0.15			
Kumtag-8	3.0896	0.848	0.001	0.850	0.002	3.643	0.003	3.635	0.006	0.22	0.19			
Kumtag ave.						3.604	0.003	3.567	0.007	0.98	0.20	H5	S2	W2
NWA 065	2.3820	0.735	0.001	0.751	0.002	3.242	0.005	3.171	0.008	2.20	0.28	H5	S2	W4
Dawn (a)	1.9645	0.574	0.001	0.587	0.002	3.424	0.007	3.350	0.010	2.18	0.36	H6		
H ave.						3.435	0.133	3.327	0.147	3.12	3.493			
Kumtag 014_1	3.3750	1.007	0.001	1.084	0.004	3.353	0.001	3.114	0.011	7.13	0.33			
Kumtag 014_2	3.3754	1.006	0.001	1.079	0.002	3.356	0.002	3.127	0.005	6.83	0.16			
Kumtag 014 ave.	6.7504	2.012	0.001	2.163	0.005	3.355	0.002	3.120	0.008	6.98	0.24	L3	S1	W2
Xincheng	2.3998	0.712	0.001	0.728	0.002	3.424	0.006	3.298	0.007	2.12	0.28	L3	S3	W3
Kumtag 017	2.9856	0.876	0.000	0.877	0.001	3.410	0.001	3.405	0.002	0.16	0.07	L5	—	W3
Kumtag 028	2.3410	0.687	0.000	0.690	0.000	3.408	0.001	3.392	0.002	0.46	0.07	L5	—	W3
Kumtag 036	5.0022	1.451	0.001	1.453	0.001	3.448	0.002	3.442	0.001	0.17	0.07	L5	—	W2
SaU 001	1.2846	0.378	0.001	0.386	0.002	3.397	0.011	3.330	0.016	2.00	0.55	L4/5	S2	W1
AM 004	2.5645	0.768	0.001	0.776	0.001	3.337	0.003	3.306	0.006	0.94	0.20	L5	S5	W2
AM 006	3.6854	1.093	0.001	1.106	0.004	3.373	0.002	3.331	0.011	1.22	0.32	L5	S5	W2
AM 014	2.5603	0.749	0.001	0.765	0.001	3.419	0.002	3.347	0.004	2.09	0.14	L5	S5	W2
AM 021	3.9839	1.176	0.001	1.188	0.001	3.387	0.003	3.355	0.002	0.94	0.12	L5	S5	W2
AM 024	4.6587	1.361	0.000	1.368	0.001	3.423	0.001	3.407	0.004	0.49	0.11	L5	S5	W2
AM 029	4.7593	1.400	0.000	1.414	0.001	3.399	0.001	3.365	0.003	1.00	0.07	L5	S5	W2
AM 033	5.4014	1.575	0.001	1.587	0.001	3.430	0.002	3.404	0.002	0.76	0.08	L5	S5	W2
AM 034	3.9848	1.162	0.001	1.163	0.001	3.430	0.002	3.427	0.004	0.09	0.12	L5	S5	W2
AM 036	4.7831	1.410	0.000	1.412	0.001	3.393	0.001	3.388	0.001	0.16	0.04	L5	S5	W2
AM 037	3.8030	1.129	0.001	1.122	0.001	3.369	0.003	3.389	0.003	-0.59	0.11	L5	Melt	W2
AM 039	2.1610	0.633	0.000	0.639	0.001	3.412	0.002	3.381	0.004	0.92	0.13	L5	S5	W2
AM 040	2.6824	0.788	0.001	0.785	0.001	3.406	0.005	3.418	0.004	-0.34	0.17	L5	S5	W2
Hami 004	3.7385	1.096	0.001	1.099	0.001	3.411	0.002	3.403	0.004	0.25	0.12	L5	S3	W2
NWA 6727	1.7508	0.515	0.001	0.526	0.002	3.402	0.003	3.326	0.011	2.24	0.35	L5	S1	W1
Tuya 003-1	4.4063	1.282	0.001	1.287	0.001	3.436	0.003	3.424	0.004	0.36	0.14	L5		
Tuya 003-2	4.2261	1.224	0.001	1.231	0.001	3.452	0.004	3.434	0.003	0.53	0.13	L5		
Tuya 003-3	3.7020	1.070	0.001	1.069	0.003	3.460	0.005	3.464	0.008	-0.09	0.27	L5		
Tuya 003-4	3.8084	1.101	0.001	1.109	0.001	3.461	0.003	3.434	0.004	0.78	0.15	L5		
Tuya 003-5	3.7706	1.083	0.001	1.095	0.002	3.480	0.002	3.443	0.006	1.08	0.18	L5		
Tuya 003-6	3.6019	1.038	0.001	1.047	0.001	3.472	0.003	3.439	0.003	0.93	0.13	L5		
Tuya 003-7	4.1963	1.212	0.001	1.219	0.001	3.463	0.003	3.443	0.002	0.57	0.11	L5		
Tuya 003 ave.	27.7116	8.010	0.008	8.057	0.010	3.460	0.003	3.440	0.004	0.58	0.15	L5		W3
Yu Wei Liang 001	3.3856	0.999	0.001	1.006	0.002	3.390	0.004	3.365	0.007	0.74	0.24	L4-6	S2	W1
L ave.						3.404	0.029	3.365	0.069	1.063	1.533			

For non-Antarctic find OCs, the grain densities of nine H OCs are in the range of 3.242±0.005 to 3.614±0.008 g/cm³, with an average of 3.435±0.133 g/cm³. The bulk densities of these eight H OCs vary from 3.171±0.008 to 3.567±0.007 g/cm³, with an average of 3.327±0.147 g/cm³. The porosities of these meteorites vary between

Table 3
Mass, Volume, Density, and Porosity Values of Measured Antarctic Ordinary Chondrites

Sample	Mass (g)	Grain volume (cm³)	1sd	Bulk volume (cm³)	1sd	Grain density (g/cm³)	1sd	Bulk density (g/cm³)	1sd	Porosity (%)	1sd	Class	Shock stage	Weathering degree
GRV 054472	2.4380	—	—	—	—	3.604	0.001	—	—	—	—	H3	S1	W1
GRV 090309	7.7133	—	—	—	—	3.453	0.008	—	—	—	—	H3	S1	W2
GRV 090334	3.3959	0.944	0.002	0.955	0.001	3.599	0.007	3.554	0.005	1.235	0.21	H3	S1	W2
GRV 020210	2.4378	—	—	—	—	3.458	0.003	—	—	—	—	H4	S2	W1
GRV 020221	4.6609	—	—	—	—	3.530	0.006	—	—	—	—	H4	S2	W1
GRV 020277	3.0291	—	—	—	—	3.568	0.005	—	—	—	—	H4	S1	W2
GRV 051951	3.8004	—	—	—	—	3.565	0.001	—	—	—	—	H4	S3	W1
GRV 090002	1.1350	0.321	0.001	0.341	0.008	3.538	0.007	3.333	0.075	5.786	2.11	H4	S1	W2
GRV 090251	3.4368	—	—	—	—	3.462	0.074	—	—	—	—	H4	S2	W1
GRV 090300	3.9072	—	—	—	—	3.370	0.007	—	—	—	—	H4	S1	W3
GRV 090303	4.1935	—	—	—	—	3.538	0.001	—	—	—	—	H4	S1	W2
GRV 090325	1.8030	0.510	0.001	0.541	0.002	3.538	0.005	3.335	0.012	5.752	0.37	H4	S1	W3
GRV 090328-1	5.7802	—	—	—	—	3.575	0.035	—	—	—	—	H4	S2	W2
GRV 090328-2	1.0542	0.289	0.001	0.303	0.001	3.648	0.009	3.484	0.010	4.494	0.37	H4	S2	W2
GRV 090331-1	4.6871	—	—	—	—	3.400	0.020	—	—	—	—	H4	S2	W2
GRV 090331-2	2.9047	0.823	0.001	0.862	0.002	3.528	0.001	3.371	0.009	4.445	0.26	H4	S2	W2
GRV 090332	3.1815	—	—	—	—	3.537	0.009	—	—	—	—	H4	S1	W2
GRV 090650	2.5455	—	—	—	—	3.552	0.003	—	—	—	—	H4	S2	W2
GRV 090708	2.7231	—	—	—	—	3.486	0.002	—	—	—	—	H4	S2	W2
GRV 090709	4.6312	—	—	—	—	3.517	0.002	—	—	—	—	H4	S2	W2
GRV 090746	2.5616	0.714	0.000	0.722	0.001	3.587	0.002	3.549	0.006	1.053	0.17	H4	S3	W2
GRV 091002-1	3.7918	—	—	—	—	3.733	0.060	—	—	—	—	H4	S2	W2
GRV 091002-2	2.2980	0.635	0.001	0.637	0.002	3.616	0.006	3.606	0.013	0.298	0.39	H4	S2	W2
GRV 091017-1	5.5172	—	—	—	—	3.585	0.017	—	—	—	—	H4	S1	W2
GRV 091017-2	3.4873	0.979	0.001	0.996	0.003	3.564	0.004	3.501	0.011	1.767	0.33	H4	S1	W2
GRV 090591	5.8522	1.687	0.001	1.800	0.006	3.469	0.001	3.251	0.011	6.272	0.32	H5	S3	W3
GRV 052320	2.8770	0.831	0.000	0.864	0.001	3.464	0.002	3.331	0.003	3.844	0.11	H5	S3	W1
GRV 054348	1.5665	—	—	—	—	3.471	0.004	—	—	—	—	H6	S2	W1
H ave.						3.536	0.077	3.432	0.121	3.49	2.22			
GRV 091001	2.5020	0.696	0.001	0.781	0.020	3.593	0.004	3.203	0.084	10.86	2.33	L3	S1	W2
GRV 091001	6.0055	—	—	—	—	3.500	0.000	—	—	—	—	L3	S1	W2
GRV 052080	3.6680	—	—	—	—	3.450	0.002	—	—	—	—	L3	S1	W1
GRV 090748	5.1630	1.509	0.001	1.513	0.002	3.422	0.004	3.413	0.004	0.26	0.14	L3	S1	W2
GRV 090298	3.6559	1.035	0.011	1.058	0.002	3.534	0.039	3.454	0.007	2.26	1.09	L4	S3	W2
GRV 090407	4.3127	—	—	—	—	3.310	0.001	—	—	—	—	L4-melt breccia		W2
GRV 090479-1	3.7488	—	—	—	—	3.325	0.032	—	—	—	—	L4	S2	W1
GRV 090479-2	4.0062	1.148	0.000	1.200	0.002	3.489	0.001	3.340	0.006	4.27	0.16	L4	S2	W1
GRV 090751	3.0043	0.867	0.001	0.875	0.027	3.465	0.002	3.432	0.106	0.97	3.06	L4	S4	W2
GRV 090863-1	3.8632	—	—	—	—	3.464	0.067	—	—	—	—	L4	S2	W1
GRV 090863-2	3.8610	1.101	0.001	1.146	0.005	3.508	0.004	3.371	0.014	3.90	0.41	L4	S2	W1
GRV 091013-1	3.1733	—	—	—	—	3.270	0.000	—	—	—	—	L4	S2	W1
GRV 091013-2	2.8331	0.823	0.001	0.865	0.003	3.442	0.003	3.276	0.010	4.84	0.30	L4	S2	W1
GRV 020576	2.2326	—	—	—	—	3.534	0.003	—	—	—	—	L5	S2	W1
GRV 022456	1.2900	—	—	—	—	3.528	0.004	—	—	—	—	L5	S4	W2
GRV 022463	2.4310	—	—	—	—	3.493	0.003	—	—	—	—	L5	S2	W1
GRV 024447	5.2466	—	—	—	—	3.422	0.002	—	—	—	—	L5	S2	W1
GRV 050047	1.9843	—	—	—	—	3.504	0.006	—	—	—	—	L5	S4	W1
GRV 050059	3.1912	—	—	—	—	3.453	0.004	—	—	—	—	L5	S3	W1
GRV 053822	4.1398	—	—	—	—	3.434	0.001	—	—	—	—	L5	S3	W1
GRV 090007	4.0074	—	—	—	—	3.494	0.003	—	—	—	—	L5	S3	W2
GRV 090008	1.3195	—	—	—	—	3.470	0.004	—	—	—	—	L5	S3	W1
GRV 090056	4.0644	—	—	—	—	3.466	0.002	—	—	—	—	L5	S2	W2
GRV 090078	2.4222	—	—	—	—	3.447	0.001	—	—	—	—	L5	S2	W2
GRV 090087	3.1031	—	—	—	—	3.427	0.004	—	—	—	—	L5	S4	W2
GRV 090088	2.0677	—	—	—	—	3.430	0.002	—	—	—	—	L5	S4	W2

Table 3 (continued)

Sample	Mass (g)	Grain volume (cm^3)	1sd	Bulk volume (cm^3)	1sd	Grain density (g/cm^3)	1sd	Bulk density (g/cm^3)	1sd	Porosity (%)	1sd	Class	Shock stage	Weathering degree
GRV 090089	2.8961	—	—	—	—	3.432	0.003	—	—	—	—	L5	S3	W2
GRV 090092	2.5977	—	—	—	—	3.416	0.001	—	—	—	—	L5	S2	W2
GRV 090093	2.542	—	—	—	—	3.477	0.004	—	—	—	—	L5	S3	W2
GRV 090105-1	5.2689	—	—	—	—	3.425	0.004	—	—	—	—	L5	S3	W2
GRV 090105-2	1.8725	0.539	0.001	0.548	0.001	3.474	0.008	3.416	0.008	1.66	0.30	L5	S3	W2
GRV 090109	4.0514	—	—	—	—	3.453	0.003	—	—	—	—	L5	S1	W2
GRV 090110	4.5670	—	—	—	—	3.465	0.003	—	—	—	—	L5	S1	W3
GRV 090111	5.1550	—	—	—	—	3.458	0.001	—	—	—	—	L5	S1	W1
GRV 090113	2.1091	—	—	—	—	3.466	0.007	—	—	—	—	L5	S4	W2
GRV 090117	2.4293	—	—	—	—	3.440	0.005	—	—	—	—	L5	S1	W2
GRV 090128	3.4496	—	—	—	—	3.482	0.001	—	—	—	—	L5	S2	W2
GRV 090142	2.6877	0.752	0.004	0.810	0.001	3.575	0.016	3.317	0.004	7.23	0.45	L5	S2	W3
GRV 090143-1	2.4751	—	—	—	—	3.393	0.094	—	—	—	—	L5	S3	W1
GRV 090143-2	2.9069	0.835	0.001	0.839	0.001	3.481	0.002	3.466	0.005	0.42	0.16	L5	S3	W1
GRV 090154-1	3.7596					3.464	0.003					L5	S2	W2
GRV 090154-2	2.5818	0.747	0.001	0.756	0.002	3.455	0.003	3.416	0.009	1.14	0.28	L5	S2	W2
GRV 090166	4.2520	—	—	—	—	3.465	0.001	—	—	—	—	L5	S2	W2
GRV 090168	3.2643	0.942	0.000	0.956	0.002	3.467	0.001	3.416	0.006	1.47	0.18	L5	S2	W2
GRV 090253-1	2.0004	—	—	—	—	3.467	0.003	—	—	—	—	L5	S3	W2
GRV 090253-2	4.5654	1.326	0.001	1.339	0.002	3.443	0.003	3.410	0.006	0.98	0.19	L5	S3	W2
GRV 090351	2.3020	—	—	—	—	3.512	0.003	—	—	—	—	L5	S3	W1
GRV 090360	3.0640	—	—	—	—	3.513	0.001	—	—	—	—	L5	S1	W1
GRV 090361	3.9265	—	—	—	—	3.433	0.002	—	—	—	—	L5	S3	W1
GRV 090368	3.5189	—	—	—	—	3.420	0.001	—	—	—	—	L5	S3	W2
GRV 090409	5.7761	—	—	—	—	3.415	0.001	—	—	—	—	L5	S2	W2
GRV 090470	3.1056	—	—	—	—	3.472	0.003	—	—	—	—	L5	S4	W2
GRV 090632	4.6893	—	—	—	—	3.411	0.004	—	—	—	—	L5	S3	W2
GRV 090647-1	3.6650	—	—	—	—	3.284	0.004	—	—	—	—	L5	S2	W2
GRV 090647-2	2.3920	0.691	0.002	0.699	0.002	3.464	0.011	3.423	0.009	1.19	0.36	L5	S2	W2
GRV 090657	3.8887	—	—	—	—	3.471	0.001	—	—	—	—	L5	S2	W1
GRV 090668	3.3320	—	—	—	—	3.442	0.002	—	—	—	—	L5	S4	W2
GRV 090670	3.0268	—	—	—	—	3.443	0.003	—	—	—	—	L5	S3	W2
GRV 090704	3.7112	—	—	—	—	3.472	0.004	—	—	—	—	L5	S3	W2
GRV 090749	4.6446	1.354	0.000	1.356	0.001	3.430	0.001	3.420	0.003	0.17	0.10	L5	S2	W2
GRV 090753	3.7150	1.085	0.012	1.100	0.001	3.424	0.037	3.376	0.003	1.39	1.05	L5	S3	W2
GRV 090755	2.3450	0.661	0.001	0.701	0.004	3.549	0.005	3.346	0.021	5.71	0.59	L5	S3	W2
GRV 090756-1	3.7918	—	—	—	—	3.321	0.001	—	—	—	—	L5	S2	W1
GRV 090756-2	1.5681	0.455	0.000	0.467	0.001	3.450	0.003	3.361	0.011	2.59	0.32	L5	S2	W1
GRV 090757	6.0933	—	—	—	—	3.490	0.062	—	—	—	—	L5	S4	W2
GRV 090758-1	4.0921	—	—	—	—	3.512	0.002	—	—	—	—	L5	S2	W2
GRV 090758-2	3.5935	—	—	—	—	3.472	0.002	—	—	—	—	L5	S2	W2
GRV 090758-3	2.4374	0.702	0.001	0.724	0.004	3.473	0.008	3.366	0.018	3.08	0.55	L5	S2	W2
GRV 090775	7.1000	—	—	—	—	3.485	0.001	—	—	—	—	L5	S3	W2
GRV 090831	2.9073	0.842	0.001	0.850	0.001	3.453	0.004	3.420	0.006	0.95	0.20	L5	S2	W2
GRV 090831	3.686	—	—	—	—	3.311	0.032	—	—	—	—	L5	S2	W2
GRV 090916	5.8939	—	—	—	—	3.423	0.003	—	—	—	—	L5	S2	W2
GRV 091015-1	3.8454	—	—	—	—	3.454	0.003	—	—	—	—	L5	S3	W2
GRV 091015-2	3.0484	0.886	0.000	0.891	0.001	3.442	0.002	3.420	0.005	0.66	0.15	L5	S3	W2
GRV 020574	4.3722	—	—	—	—	3.454	0.002	—	—	—	—	L6	S3	W2
GRV 022225	4.8735	—	—	—	—	3.447	0.001	—	—	—	—	L6	S3	W2
GRV 022233	4.1265	—	—	—	—	3.469	0.003	—	—	—	—	L6	S3	W2
GRV 051631	2.6884	—	—	—	—	3.499	0.003	—	—	—	—	L6	S5	W1
GRV 052965	1.8954	—	—	—	—	3.520	0.002	—	—	—	—	L6	S4	W1
GRV 053582	3.4386	—	—	—	—	3.443	0.003	—	—	—	—	L6	S4	W1
GRV 053583	4.7558	—	—	—	—	3.480	0.001	—	—	—	—	L6	S5	W1
GRV 090015	3.8482	—	—	—	—	3.468	0.001	—	—	—	—	L6	S2	W1
GRV 090057	3.7758	—	—	—	—	3.453	0.002	—	—	—	—	L6	S2	W1

Table 3 *(continued)*

Sample	Mass (g)	Grain volume (cm^3)	1sd	Bulk volume (cm^3)	1sd	Grain density (g/cm^3)	1sd	Bulk density (g/cm^3)	1sd	Porosity (%)	1sd	Class	Shock stage	Weathering degree
GRV 090719	4.2148	—	—	—	—	3.460	0.005					L6	S2	W1
L ave.						3.455	0.056	3.384	0.062	2.69	2.67			

0.47±0.11% and 12.01±0.32%, with an average of 3.12±3.49%. The grain densities of 22 L OCs vary from 3.337±0.003 to 3.448±0.002 g/cm^3, with an average of 3.404±0.029 g/cm^3. The bulk densities of these L OCs are in the range of 3.120±0.008 to 3.442±0.001 g/cm^3, and the average value is 3.365±0.069 g/cm^3. The porosities of these OCs range from 0 to 6.98±0.24%, with an average of 1.06±1.53%. Evidently, the densities and porosities of non-Antarctic OCs are much lower than those of the OC falls. However, the bulk densities of the non-Antarctic OCs are similar to those of the OC falls.

Among the Antarctic OCs, the grain densities of 24 H OCs vary from 3.370±0.010 to 3.733±0.060 g/cm^3, with an average value of 3.536±0.077 g/cm^3. Ten out of these 24 OCs have been measured for bulk density, and the bulk densities are in the range of 3.251±0.011 to 3.606±0.013 g/cm^3 with an average value of 3.432±0.121 g/cm^3. The porosities of the 10 OCs vary from 0.30±0.39 to 6.27±0.32%, with an average of 3.49±2.22%. The grain densities of 73 L OCs vary from 3.423±0.003 to 3.575±0.016 g/cm^3, with an average of 3.455±0.056 g/cm^3. The bulk densities of 21 (21 out of 73 had been measured for bulk densities) L OCs are in the range of 3.203±0.084 to 3.466±0.005 g/cm^3 with an average of 3.384±0.062 g/cm^3; the porosities of these 21 L OCs are in the range of 0.17±0.10% to 10.86±2.33% with a mean value of 2.69±2.67%. The grain densities, bulk densities, and porosities of the Antarctic OCs are similar to those of the non-Antarctic OCs.

3.2. Pore Morphology

A series of meteorites were selected to investigate pore morphology, including Bo Xian, Dhajala, Huaxi, Zaoyang, Enshi, Xining, Holbrook, Chelyabinsk, Xinglongquan, Zhaodong, and Gao-Guenie. In the Bo Xian chondrite, pores are much rarer in chondrules than in the matrix. Four types of pores were observed in this meteorite: (1) irregular intergrain vugs (<10 μm) among mineral grains (Figure 2a); (2) gaps between chondrules or large crystals and the surrounding fine grains (Figure 2b); (3) cracks within mineral crystals (Figure 2c); and (4) isolated tiny pores in minerals (Figure 2d). The characteristics of these pores are similar to those of Dhajala (Figures 2e and 2f), Huaxi (Figures 3a–3c), and Zaoyang (Figure 3d) meteorites.

The Xining, Holbrook, and Chelyabinsk meteorites show similar pore characteristics, occurring as intragrain cracks with the widths less than 10 μm (Figures 4a–4f). Unlike the Bo Xian, Huaxi, and Zaoyang meteorites, the intergrain pores in the Xining, Holbrook, and Chelyabinsk meteorites are very rare. The majority of the cracks in the Xining (Figures 4a and 4b), Holbrook (Figures 4c and 4d), and Chelyabinsk (Figures 4e and 4f) meteorites penetrate the mineral grains and form complex nets of cracks. Compared to the Xining and Holbrook meteorites, shock veins and maskelynite exist in the Chelyabinsk meteorite, and there is no crack within shock veins and maskelynite grains (Figure 4f). There is no maskelynite or shock vein observed in the studied sections of the Xining and Holbrook meteorites. Similar to olivine and pyroxene grains, plagioclase grains are heavily fractured in the Xining and Holbrook meteorites (Figures 4b and 4d). Unfractured shock veins and maskelynite grains might be the main reason for the Chelyabinsk meteorite having a lower porosity (7.18±0.14%) than the Xining (11.53±0.40%) and
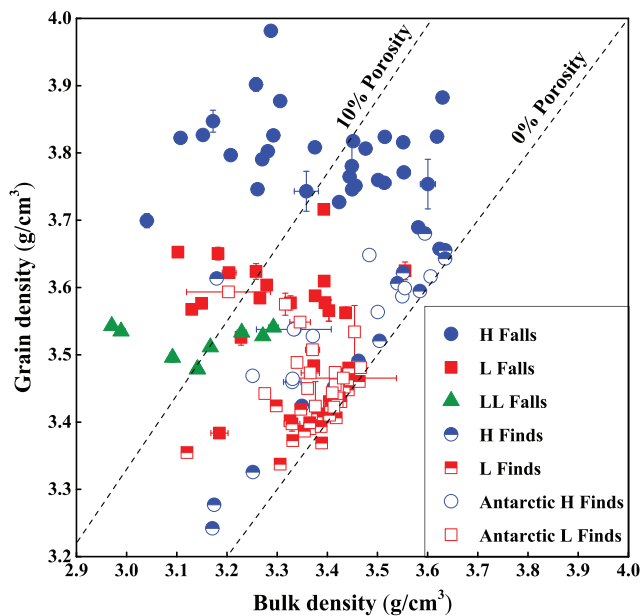
Figure 1. Bulk density versus grain density of the ordinary chondrites of falls, non-Antarctica finds, and Antarctica finds (note that the two dashed lines are the 0% porosity line and 10% line, respectively; for the majority of the data, the error bar is smaller than the size of the symbol).
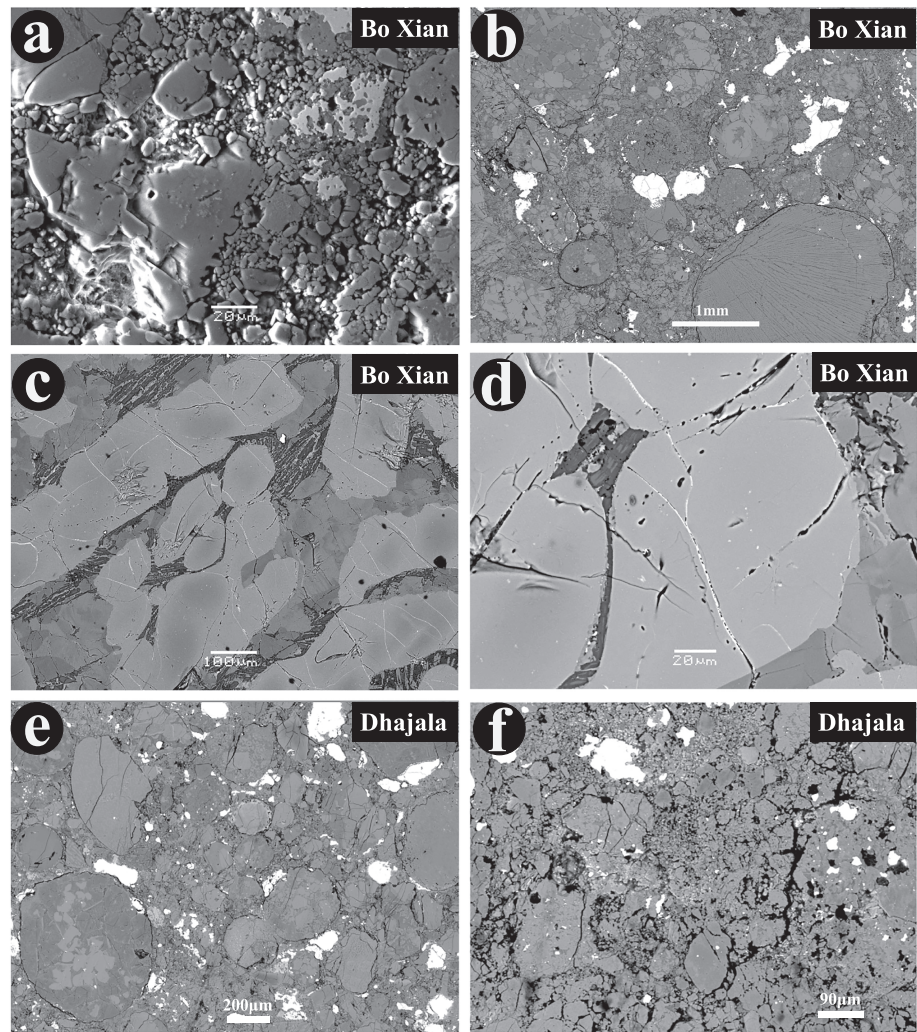
Figure 2. Secondary electron image of the Bo Xian meteorite (a), BSE images of the Bo Xian (b–d), and Dhajala (e and f) meteorites. Four major forms of pores have been observed in the two meteorites. (a) Irregular intergrain vugs among minerals in Bo Xian; (b) gaps around chondrules and large crystals; (c) cracks within minerals; (d) small isolated pores in minerals; (e) gaps around chondrules and large minerals in Dhajala; (f) intergrain vugs (black areas are vugs) in Dhajala.

Holbrook (12.10±0.10%) meteorites. The Enshi (Figures 5a and 5b) and Zhaodong (Figures 5c and 5d) meteorites have similar pore structures, but there is no shock vein in the Zhaodong meteorites. The pores in these two samples mainly exist as the form of tiny cracks with the widths less than several microns in olivine and pyroxene grains (Figures 5a–5d). Some isolated pores also occur in olivine and pyroxene grains; however, most of these pores are connected by intergrain cracks (Figures 5b and 5d). The Enshi and Zhaodong meteorites significantly differ from the Xining, Holbrook, and Chelyabinsk meteorites with smaller crack widths of mineral grains and the absence of cracks in the plagioclase grains. Intergrain cracks with widths usually less than 1 μm are the major pore morphology in the Gao-Guenie; however, most of the cracks are filled with weathering products (Figures 5e and 5f). In addition, the shock veins and shock pockets are readily seen in the observed section of the Gao-Guenie, and these veins and pockets are poreless. The tiny cracks, the cracks partially filled with weathering products, and poreless shock veins and shock pockets together make the porosity of the Gao-Guenie lower than another OC fall samples.

To investigate the effects of weathering on the porosity of OCs, available polished sections of multiple desert meteorites (Kumtag, Hami 003, and Hami 005) and Antarctic meteorites (Grove Mountains 090746 [GRV
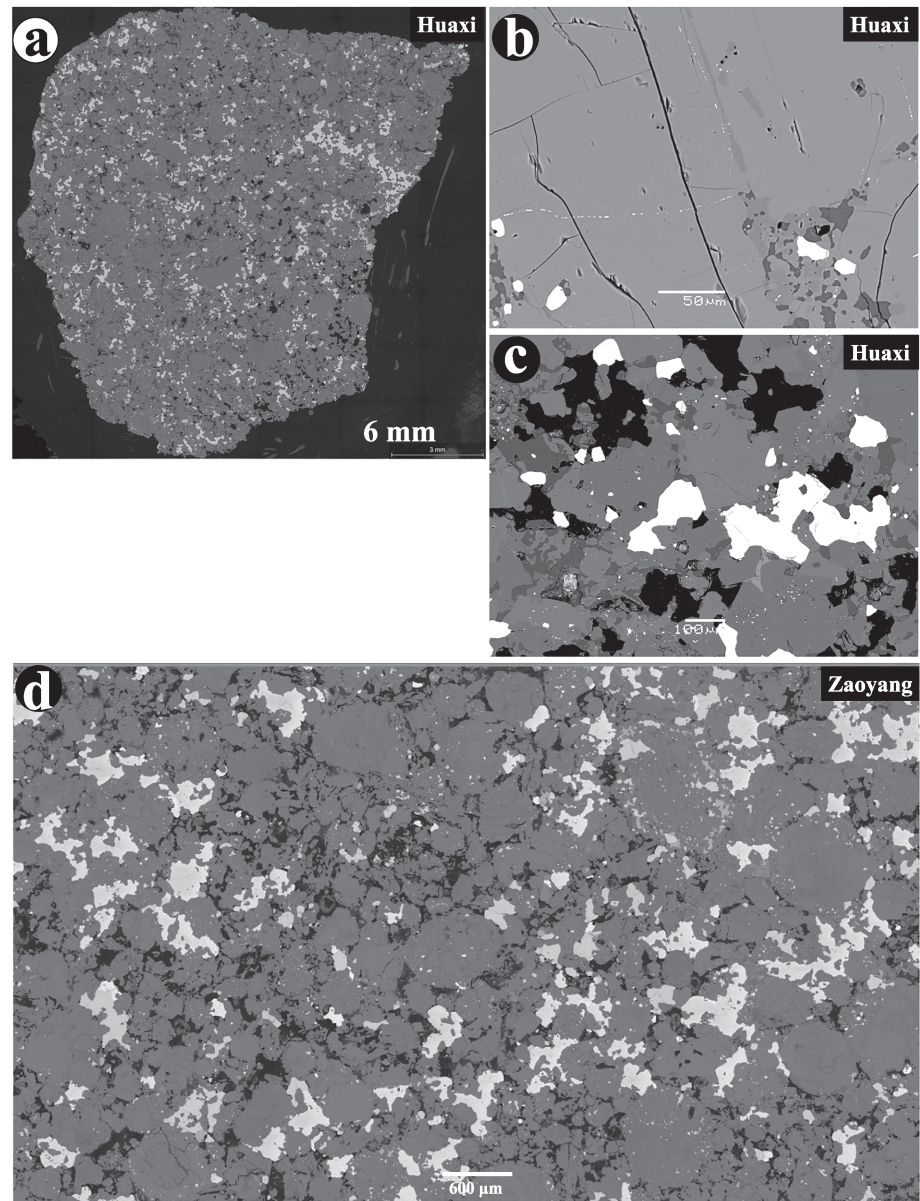
Figure 3. BSE images of the porous Huaxi (a–c) and Zaoyang (d) meteorites show four major types of pores forms similar to those in the Bo Xian and Dhajala meteorites. (a) The polished section of the Huaxi meteorites indicates that the meteorite is very porous (black dots are pores); (b) cracks and isolated tiny pores within minerals; (c) irregular intergrain vugs (black areas) are usually more than 100 μm in size; (d) structurally, the Zaoyang meteorites is similar to the Huaxi meteorites.

090746], GRV 090749, and GRV 091001) were selected. Kumtag is slightly weathered with minor rust around the kamacite crystals. The cracks in the mineral grains that surround the kamacite grains are filled with the terrestrial weathering products (Figure 6a), while these weathering products are absent in the cracks of chondrules that are separate from the kamacite (Figure 6a). Kamacite grains in Hami 003 and Hami 005 are almost altered to rust, and consequently, the cracks in the two meteorites are almost filled with weathering products (Figures 6b and 6c). The cracks in GRV 090746 and GRV 090749 are relatively rare, and most of the cracks are filled with weathering products (Figures 6d and 6e). The minerals in GRV 091001 are highly fractured, and almost no cracks are filled with weathering products (Figure 6f). The porosity of GRV 091001 is 10.86±2.33%, which is the highest porosity value among the studied Antarctic OCs.
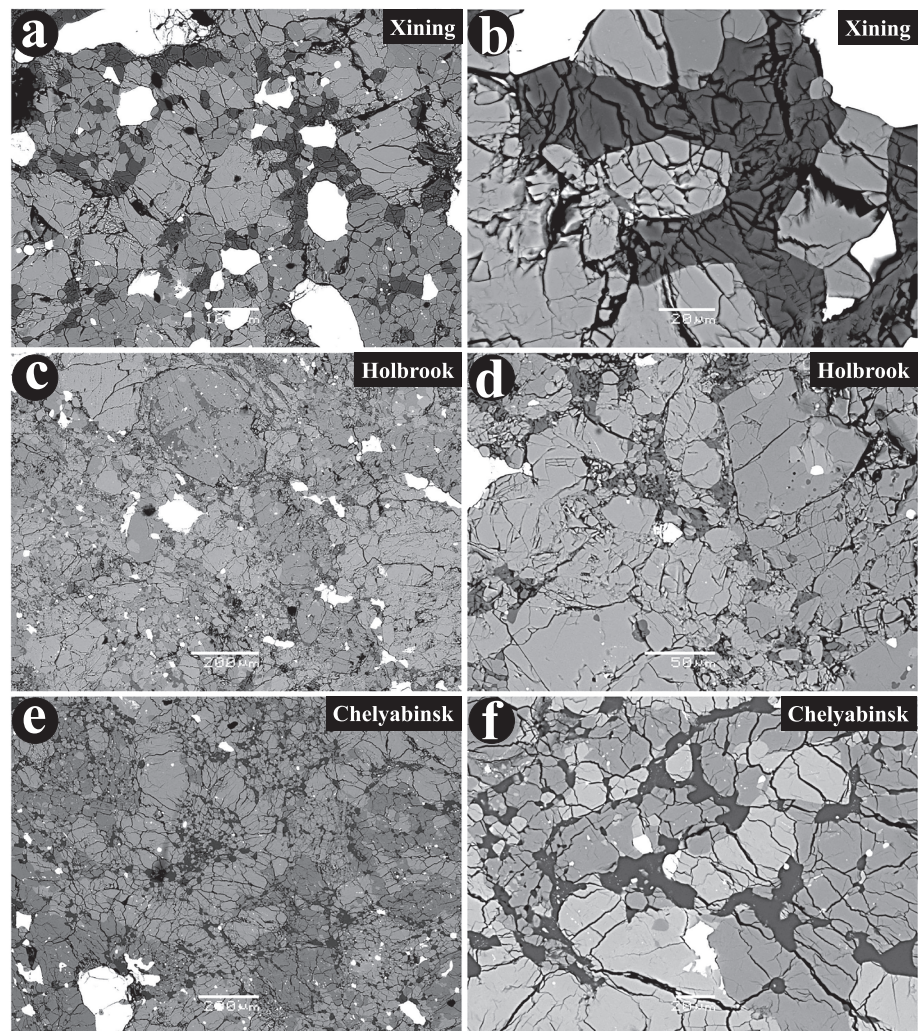
Figure 4. BSE images of the Xining (a and b), Holbrook (c and d), and Chelyabinsk (e and f) meteorites. Intergrain pores are rare, and intragrain cracks are well developed in these meteorites. All the silicate grains in the Xining (b) and Holbrook (d) meteorites are heavily fractured; however, the maskelynite grains in the Chelyabinsk meteorite (f) are intact. Note that the scale bar in image f is 20 μm.

The desert meteorites Alatage Mountain 037 (AM 037; shock melt OC) and AM 039 (S5) were selected for pore observation. The shock melt AM 037 is composed of two types of lithologies, including the crystallized lithology and the relic lithology of chondrites (Figure 7a). A few fractures are observed in this meteorite. These fractures are filled with weathering products or mineral veins (e.g., plagioclase; Figure 7b). The majority of cracks in minerals and intergrain vugs in AM 039 are mainly filled with plagioclase and minor weathering products (Figures 7d and 7e).

4. Discussion

4.1. Density, Porosity, and Weathering

For the majority of the OC falls, the influence of terrestrial weathering on their densities and porosities is negligible if these meteorites were collected shortly after the fall and preserved well. Therefore, the densities and porosities of such meteorites could represent those properties of their parent asteroid materials. The brown surface indicates that the measured fragment of the Laochenzhen is a sample with a weathering degree of W1. The surface of the Gao-Guenie fragment is disseminated by rust, and the polished section made from the same fragment confirmed the weathering degree of W1 (Figure 5e). The Guangnan was
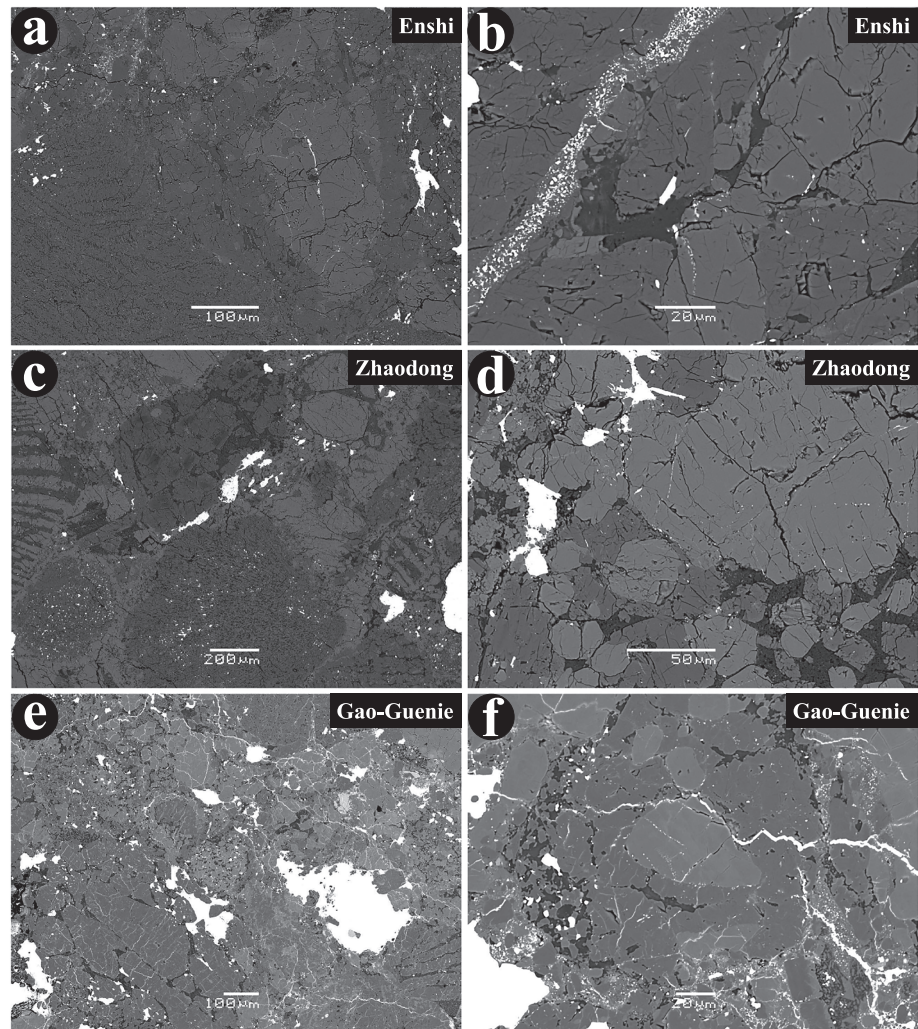
Figure 5. BSE images of the Enshi (a and b), Zhaodong (c and d), and Gao-Guenie (e and f) meteorites. The major pore forms in these meteorites are intragrain cracks (a, c, and e), and the widths of the cracks are usually less than several microns (b, d, and f). Note that most cracks in the Gao-Guenie meteorite are filled by weathering products (e and f).

reported as a moderate weathered (W2) meteorite (Wang & Rubin, 1987). Due to inappropriate preservation, the Heyetang suffered a weathering degree of W1 (Shen et al., 2013).

For these four fragments, excluding the Heyetang, which has a grain density similar to that of the L falls, the grain densities and porosities are significantly lower than those of the corresponding group falls, and the bulk densities are higher. For the OC falls, excluding the four weathered meteorites (Gao-Guenie, Laochenzhen, Guangnan, and Heyetang) in this study, the grain densities of H, L, and LL range from 3.743 ± 0.030 to 3.980 ± 0.006 g/cm^3 (average of 3.776 ± 0.062 g/cm^3), 3.384 ± 0.006 to 3.716 ± 0.005 g/cm^3 (average of 3.584 ± 0.074 g/cm^3), and 3.479 ± 0.003 to 3.541 ± 0.003 g/cm^3 (average of 3.515 ± 0.025 g/cm^3), respectively. The grain density of the Colby (Wisconsin; L6) is 3.716 ± 0.005 g/cm^3, which is much higher than those of other L group OCs in this study and almost indistinguishable from H group OCs. However, the density of a 21.819-g fragment of this meteorite measured by Macke (2010) is 3.56 g/cm^3, which is well within the range of L OCs. Therefore, we hypothesize that an Fe-Ni metal nodule is hidden in our measured Colby (Wisconsin) fragment. A fragment of Mount Tazerzait (L5) measured in this study is only 0.9982 g and the grain density is 3.384 ± 0.006 g/cm^3. The measurement of a 10.52 g Mount Tazerzait fragment gave a grain density of 2.56 ± 0.02 g/cm^3, which is a typical fresh L OC value (Sasso et al., 2009). A significantly
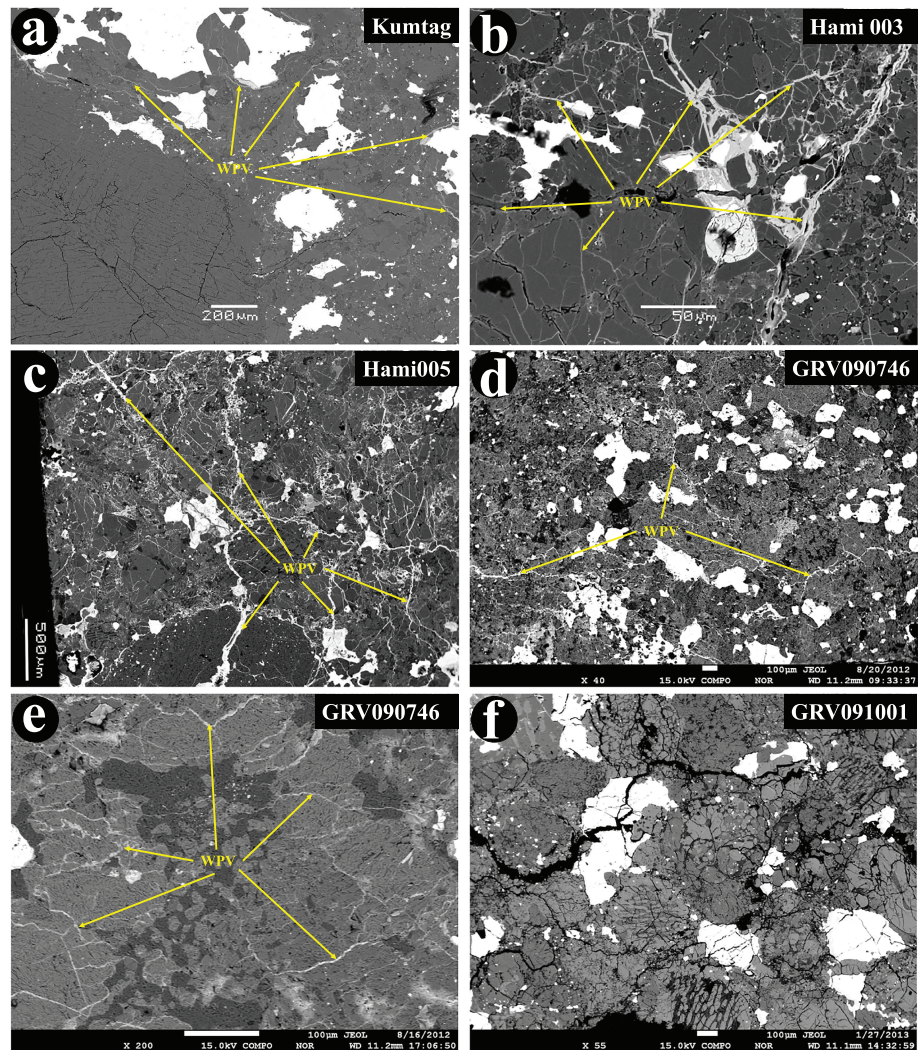
Figure 6. BSE images of some Antarctic and non-Antarctic find ordinary chondrites. The majority of the cracks in the Kumtag (a), Hami 003 (b), Hami 005 (c), GRV 090746 (d), and GRV 090749 (e) meteorites are filled by weathering products. The GRV 091001 (f) meteorite is heavily fractured, and the cracks are open. Note that scale bars in images d and f are 100 μm. WPV = weathering product veins.

lower Fe-Ni metal content might be the major reason for the notably lower grain density of Mount Tazerzait (when compared with the grain densities of six LL OCs measured in this study) in our results. The grain densities, bulk densities, and porosities of 12 Jilin fragments vary in the range of 3.727 ± 0.002 to 3.882 ± 0.007 g/cm^3, 3.375 ± 0.007 to 3.630 ± 0.002 g/cm^3, and 5.37 ± 0.10 to $11.37\pm0.0.21\%$, respectively. It seems that the bulk density is much more variable than the grain density.

For the majority of fresh OCs, the grain density ranges of H, L, and LL of falls in this study are distinguishable (Figure 1). This means that it is reliable to distinguish fresh H, L, and LL samples based on their grain densities measured from several fragments, even from fragments as small in size as 0.5 cm^3. The strong inverse correlation (Figure S1a in the supporting information) between porosities and bulk densities (this is not the case for porosities and grain densities; Figure S1b) for 31 H, 19 L, and 8 LL fragments of the OCs falls indicates that the porosities of the OCs are controlled by their bulk densities. This result is consistent with the findings of Wilkison and Robinson (2000) but contradicts the result of Wilkison et al. (2003). The masses of the OC falls in this study are in the range of 0.8953–5.6950 g, and we did not observe any correlation between porosity and sample mass (Figure S2). The observation of Consolmagno et al. (2008)
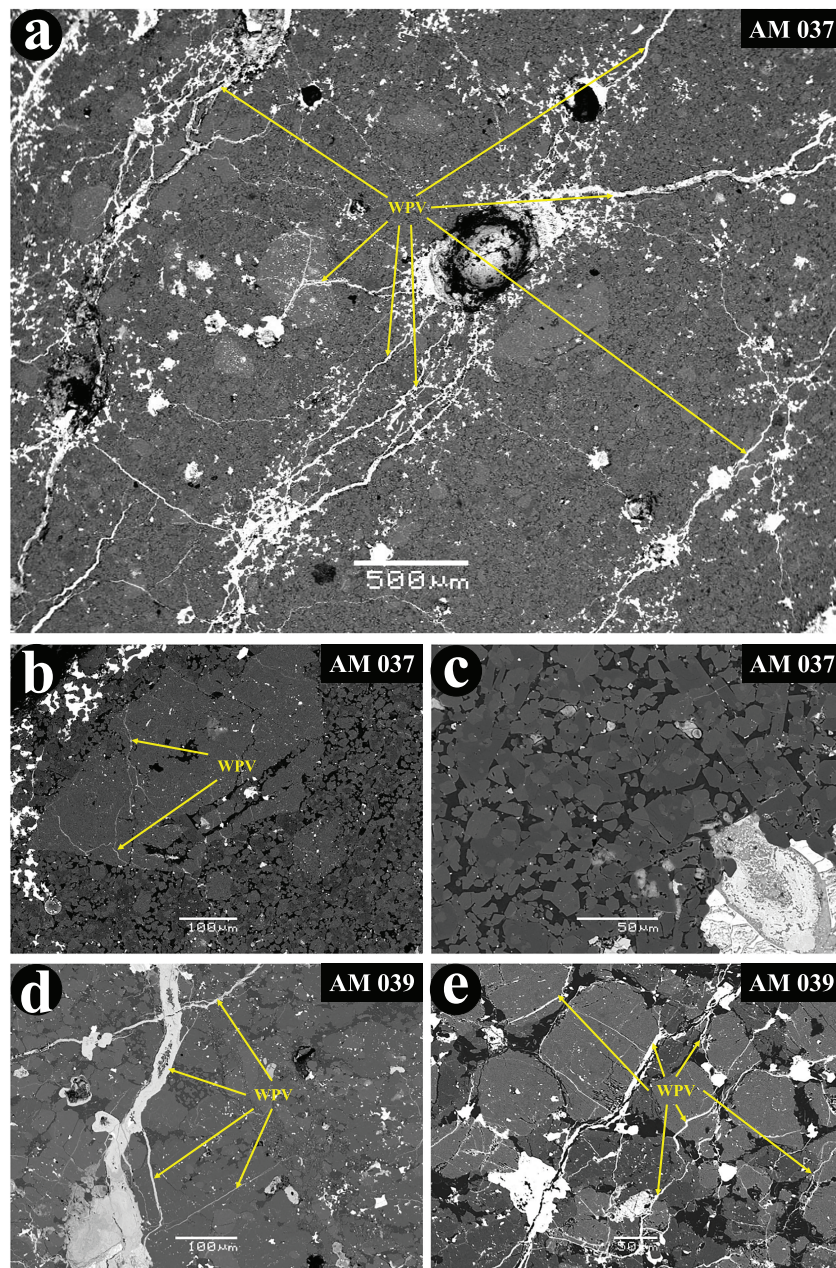
Figure 7. BSE images of some heavily shocked meteorites. (a) the AM 037 is a melt rock composed of a few relic clasts and a fine grain matrix; (b) a relic olivine surrounded by fine grain matrix; (c) the matrix part is composed of fine grain (<20 μm) minerals, and the pores are very rare. (d and e) Most cracks in the AM 039 had been filled by plagioclase during the shock process on its parent body (the scale bar in image e is 50 μm). WPV = weathering product veins. (e) Most cracks in AM 039 had been filled by plagioclase during the shock process on its parent body.

showed some weak correlations between the grain density and terrestrial age of the OC falls; however, this is not the case for our results (Figure S3a). This might indicate that the metal oxidations for the studied OC falls are negligible. We find no correlation between the porosity and terrestrial age for the studied H and L falls (Figure S3b); this means that the slow alteration of metal does not significantly change the porosity of well-preserved OCs in a period of 10 to 20 years. However, a weak inverse correlation (Figure S3b) was observed between porosity and terrestrial age in LL falls, which is probably due to the small amount of data points.

The densities and porosities of some OC falls (Gao-Guenie, Jilin, Juancheng, Zaoyang, Colby [Wisconsin], Holbrook, Mount Tazerzait, Mocs, Suizhou, and Zhaodong) have also been measured by other researchers

and are listed in Table 1. Only a few measurements are consistent with our results, these meteorites are Jilin (a 62.35-g fragment, grain density: 3.78 ± 0.04 g/cm^3; bulk density: 3.41 ± 0.03 g/cm^3; porosity: $9.8\pm0.01\%$; Beech et al., 2009), Holbrook (average of 36 fragments, grain density: 3.55 g/cm^3; bulk density: 3.18 g/cm^3; porosity: 10.4%; Macke, 2010), Mocs (average of 19 fragments, grain density: 3.63 g/cm^3; bulk density: 3.26 g/cm^3; porosity: 10.3%; Macke, 2010), and Zhaodong (a 66.32 g fragment, grain density: 3.60 ± 0.01 g/cm^3; bulk density: 3.46 ± 0.03 g/cm^3; porosity: $3.9\pm0.9\%$; Macke, 2010). However, some measurements are not in the range of our results (see Table 1). The discrepancies between literature data and our data might be due to either the heterogeneous distribution of minerals and pores or the systematic errors between different methods. Nevertheless, we are confident in the porosity measurements performed with the Pycnometer-balloon vacuum packing method. Since the bulk density and grain density of one sample are measured by the same pycnometer, the systematic errors of the two density measurements would be largely reduced.

For the Antarctic meteorites, the mean grain density of the 24 H OCs is 3.536 ± 0.077 g/cm^3, which is relatively lower than the average grain density (3.776 ± 0.062 g/cm^3) of the H falls in this study and similar to the measured six LL OCs (3.515 ± 0.025 g/cm^3). The average grain density of the 73 Antarctic L OCs is 3.455 ± 0.056 g/cm^3, which is only slightly lower than that of the 24 Antarctic H OCs measured in this study. The Antarctic L and H OCs overlap in the plot of grain density value versus bulk density value (Figure 1). Therefore, it is difficult to distinguish the two groups according to their grain densities. Similar to the OC falls, a strong correlation also exists between porosity and bulk density of the Antarctic L and H OCs (Figure S1c). However, the slopes of the best fit lines of porosity and bulk density of the Antarctic L and H OCs are different from those of the L falls and H OCs. Such differences could be related to the different amounts of metal that were oxidized during weathering processes on Earth. Interestingly, a positive correlation ($R^2=0.53$; Figure S1d) between grain densities and porosities of the Antarctic L OCs suggests that the porosity of these L OCs is mainly influenced by the weathering degree. Compared with the OC falls of the same groups, the grain densities of the Antarctic OCs are obviously smaller, while the bulk densities are slightly higher. The slightly higher bulk densities of the Antarctic OCs are in the range of the calculated results of Consolmagno et al. (2008) for the weathering effect. The influence of weathering on the porosities is clearly observed in BSE images of the Antarctic OCs. For example, the majority of the cracks of GRV 091002 and GRV 090749 are filled with weathering products (Figures 5d and 5e). The porosities of the two meteorites are 0.30% and 4.27%, respectively. Few cracks in GRV 091001 are filled with weathering products (Figure 5f), and the porosity of this sample is $10.86\pm2.33\%$.

The non-Antarctic find OCs are notably more strongly weathered than the Antarctic OCs. Almost all metal grains in most of the non-Antarctic find OCs were oxidized, and most troilite grains were partially altered. Some OCs (particularly for H) that were collected in the desert around Hami in Xinjiang, China, with the limonite agglutinates adhered to the parts that contact the ground (a similar phenomenon was also observed in the OCs collected in the Oman desert; Al-Kathiri, 2006; the same phenomenon can be observed in the Lut desert meteorites Pourkhorsandi et al., 2019). The limonite was transported by the water from the interior of the meteorite during terrestrial weathering. The strong weathering results in lower porosities and grain densities of the non-Antarctic find OCs compared to those of the Antarctic OCs. In the plots (Figures S1b, S1d, and S1) of porosity versus grain density of the OCs, the data points move to the lower left quarter with increasing weathering degrees (from falls to Antarctic finds to non-Antarctic finds). In the plots (Figures S1a, S1c, and S1e) of porosity versus grain density of the OCs, the data points slightly move toward the lower right quarter with increasing weathering degrees. It is clear that the porosities and grain densities of the OCs are more sensitive than the bulk densities of the OCs to weathering. It is also clear that the weathering degree of the non-Antarctic find OCs is usually much more severe than that of the Antarctic OCs. This is also consistent with the previous studies (Gnos et al., 2009; Li et al., 2017) in which the alteration of troilite was easily recognizable in the desert OCs but seldom found in the Antarctic OCs. It is easy to understand the weathering affecting the grain density of the OC by converting higher density metal to lower density weathering products during the entire weathering process (Consolmagno et al., 1998). The plot of the measured H OCs density values versus weathering degree (Figure S4a) clearly indicates that the grain density is inversely correlated with weathering degree. A similar inverse correlation was also observed for the L OCs (Figure S4b); however, the L OCs grain density is not as sensitive as the H OCs grain density to weathering degree. This might be due to the different Fe-Ni metal contents in the two groups. The influence of

weathering on the H OCs and L OCs is much more similar (Figures S4c and S4d). The porosity of the OCs rapidly decreases during the alteration from W0 to W1. (Figures S4c and S4d). Weathering degrees heavier than W2 do not seem to decrease the OC porosity (Figures S4c and S4d), although more samples are needed to confirm this result.

Consolmagno et al. (1998) compared the porosities of the Antarctic OCs, OC falls, and non-Antarctic OCs and found that the average porosity of the Antarctic OCs was much higher than that of the OC falls and non-Antarctic OCs. The authors concluded that the different methods, the unique low-temperature environment of Antarctica, and the artificial treatment of the samples could all be possible reasons for the Antarctic OCs to have the highest porosities compared to the other collections (Consolmagno et al., 1998). The results of the measurements in Matsui et al. (1980) and Yomogida and Matsui (1981) show that the grain densities of measured Antarctic OC samples are similar to or higher than those of the OC falls (Beech et al., 2009; Consolmagno et al., 2006; Consolmagno & Britt, 1998). The grain densities of the Allan Hills A77288 (ALHA 77288; H6) and ALHA 77249 (H5) meteorites are 3.77 and 3.84 g/cm^3, respectively, and the grain densities of the ALHA 78103 (L6), ALHA 78251 (L6), and Meteorite Hills A78003 (MET 78003; L6) meteorites are 3.73, 3.70, and 3.61 g/cm^3, respectively (Matsui et al., 1980; Yomogida & Matsui, 1981). The grain densities of the ALHA 76009 (L6) and ALHA 77231 (L6) meteorites are 3.59 and 3.58 g/cm^3, respectively. Generally, the OCs collected from Antarctica are more or less affected by weathering; therefore, the grain densities should be lower than those of the OC falls. The grain densities of meteorites in the studies of Matsui et al. (1980) and Yomogida and Matsui (1981) were measured using a helium ideal gas pycnometer, while bulk densities were measured by applying different methods. Yomogida and Matsui (1981) calculated the bulk densities of the ALHA 76009 and ALHA 77231 meteorites by using different amounts of clay to wrap the meteorites that were then placed into the water so that the volumes of the measured meteorites could be extrapolated. By doing so, the porosities of the ALHA 76009 and ALHA 77231 meteorites were calculated to be 19.4% and 14.3%, respectively (Yomogida & Matsui, 1981). Matsui et al. (1980) processed the meteorites into regular cuboids; then, their bulk volumes were measured, and their bulk densities were calculated. The bulk densities of the three L meteorites (ALHA 78103, ALHA 78251, and MET 78003) are 3.22, 3.23, and 3.33 g/cm^3, respectively, and finally, the porosities of the three samples were obtained as 13.2%, 13.4%, and 7.8%, respectively (Matsui et al., 1980). Thus, the superposition of systematic errors in grain density and bulk density measurements may lead to higher porosities for these Antarctic meteorites.

4.2. Influence of Thermal Metamorphism on Pore Morphology

Previous studies indicated that there was no correlation between the porosity and petrographic type of OC falls (Consolmagno et al., 2008; Macke, 2010). The OC falls with low petrographic types are rare in this study; they are mainly type 5 or type 6. Therefore, the relationship between petrographic type and porosity is beyond the scope of this work. Here, we only investigated the changes in pore occurrences with increasing thermal metamorphism increasing. Type 3 chondrites suffered less thermal metamorphism than chondrites with higher petrographic types (Dodd et al., 1967; Grossman & Brearley, 2005; Wood, 1967). In addition, type 3 OCs also tend to have lower shock degrees (Stöffler et al., 1991). Consequently, the pore occurrences within less shocked type 3 chondrites were retained to a greater extent as the time of chondrite parent body formation. Type 5 and type 6 chondrites have been thought to be the thermal metamorphism products of lower petrographic types of the same group (Dodd, 1969; Schaefer & Fegley, 2009). We can assume that the voids in the OCs as a certain mineral phase, which is unavoidably affected by thermal metamorphism. The differences in pore occurrences between less shocked type 3 and less shocked type 5–6 OCs could be the consequences of thermal metamorphism.

We investigated three sections of type 3 OC falls (LL3 Bo Xian, H3 Dhajala, and L3 Xinglongquan). Sharply defined chondrules and clear boundaries between chondrules and the matrix indicated that the structures of the meteorites were not disturbed by a later process after their formation. In the three meteorites, in addition to the cracks within minerals created from impact, the majority of pores existed as vugs between matrix grains and as gaps between chondrules or large crystals and the surrounding fine grains (Figures 2a, 2b, 2e, and 2f). To a large extent, the vugs and gaps in type 3 chondrites should form the condensation of the parent material.

We have a type 5 chondrite Huaxi, which has been considered to be a less compacted meteorite (Li, et al., 2017). This means that the vugs between minerals and as gaps between chondrules or large crystals and
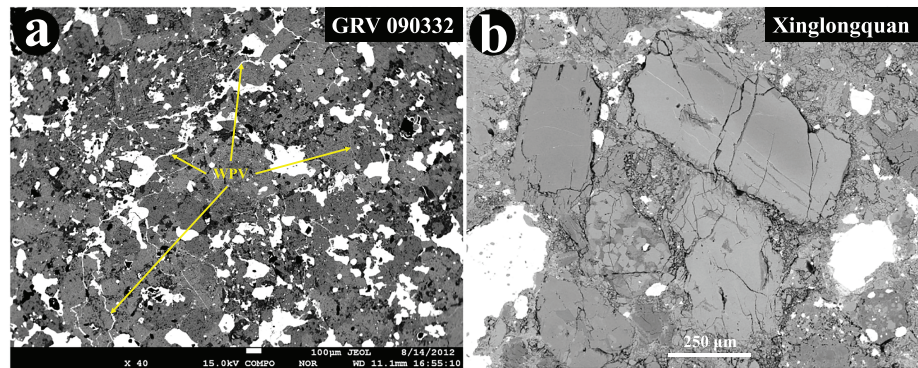
Figure 8. The GRV 090332 (a; the scale bar is 100 μm) and Xinglongquan (b) meteorites are chondrites with shock degrees of S1, and intragrain cracks are rare in minerals of these two meteorites. The widths of these cracks are usually less than several microns and mainly in grains of olivine and pyroxene. WPV = weathering product veins.

the surrounding grains in Huaxi are mainly affected by thermal metamorphism after their parent body formation. Comparing type 5 Huaxi with the type 3 chondrites Bo Xian, Dhajala, and Xinglongquan, we can conclude that pores would act as minerals: merging and growing. This means that during thermal metamorphism of OC materials, small pores will merge and become larger.

4.3. Shock Influence on Porosity

Impact played a significant role during the evolution of the OC parent bodies by generating many effects on the materials of OCs. Stöffler et al. (1991) reported various effects that were recorded in the minerals of OCs. Among these effects, irregular fractures in silicates and troilite are the most universal phenomena. Experimental studies indicated that the porosities of porous water-bearing sandstones would decrease considerably to zero porosity under 0.2 to 0.9 GPa to ~3 GPa and ~3 to ~5.5 GPa shock loadings (Stöffler, 1984; Stöffler & Grieve, 2007). The shock experiment of dry Seeberger sandstone with 25–30% porosity demonstrated that the intergrain pores disappeared during collapse and that some of them were transformed into intragrain cracks under 2 GPa shock loading (Figure 2a and 2b in Kowitz et al., 2013).

The GRV 090332 and Xinglongquan meteorites are chondrites with shock degrees of S1, and intragrain cracks are rare in minerals of these two meteorites. The widths of these cracks are usually less than several microns and mainly in grains of olivine and pyroxene (Figures 8a and 8b). The intergrain vugs are the major form of pores (Figures 8a and 8b). All of these pore characteristics of the S1 OCs were also observed in the Kernouve (H6, S1; see Figures 1 and 2 in Friedrich et al., 2013).

For meteorites with shock degrees of S2 (Holbrook, GRV 090251, GRV 090078, and GRV 090756), the intragrain cracks are denser and wider than those in the OCs with S1 shock degrees. The cracks appear in all kinds of silicate minerals and troilite grains, and most of cracks penetrate a number of mineral grains to form a crack network in the thin sections (e.g., Figure 4c). In the sections of the S3 OCs, such as Xining, Zhaodong, Gao-Guenie, GRV 090775, GRV 090591, GRV 090143, and GRV 090719, the intragrain cracks are well developed and connected into a network in each section (e.g., Figure 4a). The shock veins occur in some of the S3 OCs, and the micron-sized pores are very rare in such shock veins. Therefore, the appearance of a shock vein can reduce the porosity of the OCs. The porosity measurement might also confirm this, since in this study, there are no meteorites with porosities over 10.0% in the 12 OC falls with shock veins, and the average porosity of the ten fresh OCs is 7.227±1.778%. The average porosity of the 23 fresh OC falls free of shock veins is 10.97±4.037%. For the S4 OCs, such as Suizhou, Chelyabinsk, and Enshi, shock veins occur in all samples, and the intragrain cracks are very dense in olivine and pyroxene grains, while cracks are very rare in plagioclase grains (e.g., Figures 4a and 5a). Most plagioclase grains in Suizhou and Chelyabinsk had been transformed into maskelynite surrounded by radial cracks in the surrounding olivine and pyroxene grains (e.g., Figure 4f; Figures 2 and 4 in Xie et al., 2001). The AM 039 meteorite is the only S5 OC investigated using SEM in this study, and the spaces between the olivine and pyroxene grains are filled with plagioclase (Figure 7d). The intragrain cracks are very rear and usually occupied by plagioclase or troilite (metal; Figure 7e). For the shock melt meteorite AM 037, the intragrain cracks are very rare (Figure 7c), and the

Table 4
Calculation of Porosities of Some S-Type Asteroids

Object	Density (g/cm^3)	Mass (kg)	Asteroid class	Porosity (%)[a]	Porosity (%)[b]	Ref.
11 Parthenope	2.72±0.12	5.13 x 10^{18}	S	28.3±4.1	22.6±4.0	1
20 Massalia	3.26±0.6	5.25 x 10^{18}	S	14.1±16.9	7.3±17.7	2
243 Ida	2.7±0.4	4.20 x 10^{16}	S	28.8±11.4	23.2±11.9	3
433 Eros	2.67±0.03	6.68 x 10^{15}	S	29.6±1.7	24.0±1.4	4
3749 Balam	1.2±0.6	1.50 x 10^{14}	S	68.4±16.2	65.9±17.3	5
25143 Itokawa	1.95±0.14	3.58 x 10^{10}	S	48.6±4.3	44.5±4.4	6
1991 VH	1.6±0.5	1.50 x 10^{12}	S	57.8±13.7	54.5±14.5	7
1999 KW4	1.97±0.24	2.33 x 10^{12}	S	48.1±7.0	44.0±7.2	8
4179 Toutatis	2.1-2.5	5.05 x 10^{13}	S	34.1-44.6	28.9-40.3	9 and 10

Note. References: 1 = Viateau and Rapaport (1997); 2 = Bange (1998); 3 = Petit et al. (1997); 4 = Yeomans et al. (2000); 5 = Marchis et al. (2005); 6 = Abe et al. (2006); 7 = Rabinowitz et al. (2005); 8 = Ostro et al. (2006); 9 = Scheeres et al. (1998); 10 = Huang et al. (2013).
[a]Porosity of asteroid calculated using average grain density of H OC in this study. [b]Porosity of asteroid calculated using average grain density of LL OC in this study.

cracks in relic breccia are mainly filled with plagioclase (Figure 7b). It is clear that the heavy shock loading significantly compacts the heavy shock samples and destroys any intergrain vugs but creates a few intragrain cracks.

Based on the information given above, the OCs with different shock degrees show different pore characteristics. In the OCs with a shock degree of S1, the pores are mainly intragrain cracks in minerals (Figure 2c), as well as gaps between chondrules or large crystals and the surrounding fine grains (Figure 2b), and shock-induced cracks are rare within mineral grains. In the OCs with an S2 shock degree, pores mainly occur as intragrain cracks in mineral grains (except Fe-Ni metal), with most of the cracks connecting to form a network. The minerals present in OCs of shock degree S3 are much more fractured, and shock-melt veins sometimes occur. Cracks and irregular pores are relatively rare in shock-melt veins. Intergrain cracks and vugs are also rare in S3 OCs. The pore characteristics of S4 OCs are similar to those of S3 OCs; however, shock-melt veins are common in all S4 OCs. In addition, maskelynite can be seen in S4 OCs, for example, in the Chelyabinsk and Suizhou (Chen et al., 2004; Xie et al., 2001; Xu et al., 2016). For S5 and S6 OCs, significant shock melt occurs, and the cracks in olivine and pyroxene grains are filled by melted plagioclase glass. The majority of cracks are erased by recrystallization, which is a consequence of shock heat. Therefore, we can conclude that the pore characteristics of the OCs were significantly affected by the impact(s) on asteroid parent bodies.

For the OC falls with shock degrees over S2 in this study, the porosities decrease with increasing shock degree (Figure S5). The lowest porosities are 11.57±0.24%, 4.57±0.56%, and 3.54±0.31% for the OCs with shock degrees of S2, S3, and S4, respectively. For an OC with a shock degree higher than S3, its porosity is significantly decreased by shock compression as well as the occurrence of shock veins, shock pockets, shock melt, and maskelynite (e.g., Gao-Guenie, Jilin, Chelyabinsk, and Suizhou). The shock experiment of a sandstone with 26% porosity indicated that the decreasing porosity and formation of intragrain cracks are on the cost of intergrain pores (Kowitz et al., 2013). Previous studies also indicated that the porosity of OCs is anticorrelated with their shock degrees (Consolmagno et al., 1998; Macke, 2010). The shock transition from S1 to S2 results in an increase in the measured porosity by creating some irregular cracks that link the isolated pores with the open pores (instead of compressing the porosity). Therefore, we can conclude that the shock degree over S2 on the parent asteroid of the OCs decreases the porosity of the rock material.

4.4. Friability of OCs

Many authors have shown interest in friable meteorites (Flynn et al., 1999; Merrill & Stokes, 1900; Wilkison et al., 2003). Flynn et al. (1999) inferred that the highly friable porous meteorites may appear to have originated from low-density asteroids. However, the extremely friable meteorite does not always have very high porosity. During sample preparation, we found that the Xining meteorite (11.53% porosity) is extremely friable (e.g., can be powdered by thumb and finger). The Huaxi meteorite is more nonfriable than Xining meteorite, although it also has a higher porosity of 17.61±0.23% (Li et al., 2017). The Holbrook (12.10 ±0.11% porosity) and Chelyabinsk meteorite (7.18±0.14% porosity) are also much more friable than the

Huaxi meteorite. Our studies have shown that pore morphology plays a significant role in controlling the friability of OCs. The well-developed intracracks make the OC materials much more friable.

4.5. Implication of Macropores in Some Asteroids

The highest porosity of OC meteorite measured in this study was 17.61±0.23%. The highest porosity of OC falls measured in previous works are 26.6±0.9% (Eichstädt, H5) and 26.6±1.1% (Sena, H4; the largest value is 27.1±11.7% for Allegan; however, the error is very large; Wilkison et al., 2003; Macke, 2010). These results indicate that the porosity of the S-type asteroid should be less than 30% if the OC represents the composition and texture of the S-type asteroid. However, the bulk densities of the S-type asteroids (Table 4) are usually much lower than the bulk densities of the OCs. We calculated the porosities of some S-type asteroids based on their estimated bulk densities and the measured average grain density of S-type asteroid OC analogs (fresh H OCs and LL OCs in this study; Table 4). By doing so, we found the porosities of most of the S-type asteroids to be significantly higher than those of their analogues H OCs or LL OCs (average porosities are 39.7% vs. 11.09% for S-type asteroids and H OCs, respectively; Table 4). It is safe to believe that the OC falls could cover all porosities of the OC materials that entered the Earth's atmosphere. Very high porosity meteorites (e.g., the porosity of CI2 meteorite Tagish Lake is up to 45%; Hildebrand et al., 2006) survived during their atmospheric entry. Therefore, if S-type asteroids are constructed by OC materials in surfaces and inner parts, then a significant amount of macropores should exist in asteroids such as 3749 Balam, 25143 Itokawa, 1991 VH, 1999 KW4, and 4179 Toutatis. Therefore, the high porosities (over 34%) indicates that asteroids are rubble-pile bodies. The porosities of the 11 Parthenope, 243 Ida, and 433 Eros are between 20% and 30% if the analog materials are OCs (Table 4). Their porosities are comparable to those of high porosity OC analogues (e.g., H5 Eichstadt and H4 Sena OCs; Macke, 2010). Therefore, it is very likely that the 11 Parthenope, 243 Ida, and 433 Eros meteorites are probably covered by rubbles. The bulk density of the 20 Massalia is very high when compared with other S-type asteroids (Table 4). If the H OCs or the LL OCs are the analog materials of the 20 Massalia, the porosities are 14.1±16.9% or 7.3±17.7%, respectively. The porosity of the 20 Massalia is similar to that of the OC falls measured in this study and other studies (Britt & Consolmagno, 2003, and the references therein; Macke, 2010). Thus, the 20 Massalia might be an intact asteroid.

5. Conclusions

1. In this study, the ranges of grain density, bulk density, and porosity of 12 fresh H OC falls are 3.743±0.030 to 3.890±0.006 g/cm^3 (average of 3.796±0.047 g/cm^3), 3.158±0.003 to 3.600±0.015 g/cm^3 (average of 3.371±0.151 g/cm^3), and 4.08±0.72–17.61±0.23% (average of 11.09±4.66%), respectively. The corresponding values for 15 fresh L OC falls are 3.384±0.006 to 3.716±0.005 g/cm^3 (average of 3.588±0.073 g/cm^3), 3.102±0.007 to 3.437±0.008 g/cm^3 (average of 3.279±0.106 g/cm3), and 3.54±0.31% to 15.07±0.22% (average of 8.58±3.32%), respectively. The values of equivalents of 6 LL OC falls are 3.479±0.003 to 3.541±0.003 g/cm^3 (average of 3.515±0.025 g/cm^3), 2.975±0.004 to 3.293±0.010 g/cm^3 (average of 3.147±0.107 g/cm^3), and 7.18±0.14% to 15.98±0.13% (average of 10.47±3.06%), respectively. The measured data indicate that one of the reliable ways to classify the chemical groups of OCs could be by using the grain densities.
2. The weathered OCs are not suitable for porosity investigations.
3. Non-Antarctic finds usually suffer significant terrestrial weathering, which results in dramatic decreases in grain densities and porosities. The average porosity of the Antarctic meteorites is higher than that of the non-Antarctic finds and lower than that of OC falls.
4. In the petrographic type 3 chondrites, pores mainly occur as intergrain pores in the matrix or as vugs between the matrix and chondrules or large crystals. Pores are very rare within the chondrules or mineral crystals. During thermal metamorphism, small pores merged as larger pores, and porosity changed slightly.
5. Very weak shock (S1 and S2) of an OC can generate small cracks in minerals that connect some isolated pores with other linked pores and may increase the measurable porosity of a meteorite. Shock intensity over S3 will compact porosities in OCs and partially transform noncrack pores into cracks.
6. For meteorites with relatively lower shock stages of S1 and S2, the pores mainly occur as irregular cracks among mineral fragments, chondrules, and the matrix surrounding the chondrules. The pores exist mainly as cracks in mineral crystals in heavily shocked meteorites (with a shock stage of ≥S3).

7. Pore morphology plays a significant role in controlling the friability of OCs; well-developed intracracks make the OC materials more friable.

8. By comparing the bulk density of a meteorite and an asteroid, the asteroid structure (e.g., rubble-pile structure and only boulders on the surface) could be inferred.

References

Abe, S., Mukai, T., Hirata, N., Barnouin-Jha, O. S., Cheng, A. F., Demura, H., et al. (2006). Mass and local topography measurements of Itokawa by Hayabusa. *Science*, *312*(5778), 1344–1347. https://doi.org/10.1126/science.1126272

Alexeyeva, K. N. (1958). Physical properties of stony meteorites and their interpretation based on the hypothesis on the origin of meteorites (in Russian). *Meteoritika*, *16*, 67–77.

Al-Kathiri, A. (2006). *Studies on Oman meteorites*. Ph D. Dissertation. Bern: Universität Bern.

Bange, J. (1998). An estimation of the mass of asteroid 20-Massalia derived from the Hipparcos minor planets data. *Astronomy and Astrophysics*, *340*, L1–L4.

Beech, M., Coulson, I. M., Nie, W., & McCausland, P. (2009). The thermal and physical characteristics of the Gao-Guenie (H5) meteorite. *Meteoritics & Planetary Science*, *57*(7), 764–770. https://doi.org/10.1016/j.pss.2009.01.002

Britt, D. T., & Consolmagno, G. J. (2000). The porosity of dark meteorites and the structure of low albedo asteroids. *Icarus*, *146*(1), 213–219. https://doi.org/10.1006/icar.2000.6374

Britt, D. T., & Consolmagno, G. J. (2003). Stony meteorite porosities and densities: A review of the data through 2001. *Meteoritics & Planetary Science*, *38*(8), 1161–1180. https://doi.org/10.1111/j.1945-5100.2003.tb00305.x

Britt, D. T., Yeomans, D., Housen, K., & Consolmagno, G. J. (2002). Asteroid density, porosity, and structure. In W. F. Bottke, et al. (Eds.), *Asteroids III* (pp. 485–500). Tucson: Univ. of Ariz. Press.

Chen, M., Xie, X. D., & El Goresy, A. (2004). A shock-produced (Mg,Fe)SiO$_3$ glass in the Suizhou meteorite. *Meteoritics & Planetary Science*, *39*(11), 1797–1808. https://doi.org/10.1111/j.1945-5100.2004.tb00076.x

Consolmagno, G. J., & Britt, D. T. (1998). The density and porosity of meteorites from the Vatican collection. *Meteoritics & Planetary Science*, *33*(6), 1231–1241. https://doi.org/10.1111/j.1945-5100.1998.tb01308.x

Consolmagno, G. J., Britt, D. T., & Macke, R. J. (2008). The significance of meteorite density and porosity. *Chemie der Erde-Geochemistry*, *68*(1), 1–29. https://doi.org/10.1016/j.chemer.2008.01.003

Consolmagno, G. J., Britt, D. T., & Stoll, C. P. (1998). The porosities of ordinary chondrites: models and interpretation. *Meteoritics & Planetary Science*, *33*(6), 1221–1229. https://doi.org/10.1111/j.1945-5100.1998.tb01307.x

Consolmagno, G. J., Macke, R. J., Rochette, P., Britt, D. T., & Gattacceca, J. (2006). Density, magnetic susceptibility, and the characteri-zation of ordinary chondrite falls and showers. *Meteoritics & Planetary Science*, *41*(3), 331–342. https://doi.org/10.1111/j.1945-5100.2006.tb00466.x

Corrigan, C. M., Zolensky, M. E., Dahl, J., Long, M., Weir, J., Sapp, C., et al. (1997). The porosity and permeability of chondritic meteorites and interplanetary dust particles. *Meteoritics & Planetary Science*, *32*(4), 509–515. https://doi.org/10.1111/j.1945-5100.1997.tb01296.x

Coulson, I. M., Beech, M., & Nie, W. (2007). Physical properties of Martian meteorites: Porosity and density measurements. *Meteoritics & Planetary Science*, *42*(12), 2043–2054. https://doi.org/10.1111/j.1945-5100.2007.tb01006.x

Dodd, R. T. (1969). Metamorphism of the ordinary chondrites: A review. *Geochimica et Cosmochimica Acta*, *33*(2), 161–203. https://doi.org/10.1016/0016-7037(69)90138-0

Dodd, R. T., & Jarosewich, E. (1979). Incipient melting in and shock classification of L-group chondrite. *Earth and Planetary Science Letters*, *44*(2), 335–340. https://doi.org/10.1016/0012-821X(79)90181-X

Dodd, R. T., van Schmus, W. R., & Koffman, D. M. (1967). A Survey of the unequilibrated ordinary chondrites. *Geochimica et Cosmochimica Acta*, *31*(6), 921–951. https://doi.org/10.1016/0016-7037(67)90071-3

Flynn, G. J., Moore, L. B., & Klock, W. (1999). Density and porosity of stone meteorites: Implications for the density, porosity, cratering, and collisional disruption of asteroids. *Icarus*, *142*(1), 97–105. https://doi.org/10.1006/icar.1999.6210

Friedrich, J. M., Macke, R. J., Wignarajah, D. P., Rivers, M. L., Britt, D. T., & Ebel, D. S. (2008). Pore size distribution in an uncompacted equilibrated ordinary chondrite. *Planetary and Space Science*, *56*(7), –895, 900. https://doi.org/10.1016/j.pss.2008.02.002

Friedrich, J. M., & Rivers, M. L. (2013). Three-dimensional imaging of ordinary chondrite microporosity at 2.6 μm resolution. *Geochimica et Cosmochimica Acta*, *116*(1), 63–70. https://doi.org/10.1016/j.gca.2011.08.045

Friedrich, J. M., Rubin, A. E., Beard, S. P., Swindle, T. D., Isachsen, C. E., Rivers, M. L., et al. (2014). Ancient porosity preserved in ordinary chondrites: Examining shock and compaction on young asteroids. *Meteoritics & Planetary Science*, *49*(7), 1214–1231. https://doi.org/10.1111/maps.12328

Friedrich, J. M., Ruzicka, A., Rivers, M. L., Ebel, D. S., Thostenson, J. O., & Rudolph, R. A. (2013). Metal veins in the Kernouve (H6 S1) chondrite: Evidence for pre- or syn-metamorphic shear deformation. *Geochimica et Cosmochimica Acta*, *116*(1), 71–83. https://doi.org/10.1016/j.gca.2013.01.009

Fujiwara, A., Kawaguchi, J., Yeomans, D. K., Abe, M., Mukai, T., Okada, T, et al. (2006). The rubble-pile asteroid Itokawa as observed by Hayabusa. *Science*, *312*(5778), 1130–1134. https://doi.org/10.1126/science.1125841

Gnos, E., Lorenzetti, S., Eugster, O., Jull, A. J. T., Hofmann, B. A., Al-Kathiri, A., et al. (2009). The Jiddat al Harasis 037 strewn field, Sultanate of Oman. *Meteoritics & Planetary Science*, *44*(3), 375–387. https://doi.org/10.1111/j.1945-5100.2009.tb00739.x

Grossman, J. N., & Brearley, A. J. (2005). The onset of metamorphism in ordinary and carbonaceous chondrites. *Meteoritics & Planetary Science*, *40*(1), 87–122. https://doi.org/10.1111/j.1945-5100.2005.tb00366.x

Herd, R. K., Miller, S. J., & Christie, I. (2003). Measurement of a meteorite volume using a non-contact 3D laser scanner, Annual Meteoritical Society Meeting, *66*, 5285.

Hildebrand, A. R., McCausland, P. J. A., Brown, P. G., Longstaffe, F. J., Russell, S. D. J., Taglianferri, E., et al. (2006). The fall and recovery of the Tagish Lake meteorite. *Meteoritics & Planetary Science*, *41*(3), 407–431. https://doi.org/10.1111/j.1945-5100.2006.tb00471.x

Huang, J. C., Ji, J., Ye, P., Wang, X., Yan, J., Meng, L., et al. (2013). The Ginger-shaped Asteroid 4179 Toutatis: New observations from a successful flyby of Chang'e-2. *Scientific Reports*, *3*(1), 3411. https://doi.org/10.1038/srep03411

Huang, Q., & Wieczorek, M. A. (2012). Density and porosity of the lunar crust from gravity and topography. *Journal of Geophysical Research*, *117*, E05003. https://doi.org/10.1029/2012JE004062

Keil, K. (1962). Quantitav-erzmikroskopische integrationsanalyse der chondrite. *Chemie der Erde*, *22*, 281–348.

Kiefer, W. S., Macke, R. J., Britt, D. T., Irving, A. J., & Consolmagno, G. J. (2012). The density and porosity of lunar rocks. *Geophysical Research Letters*, *39*, L07201. https://doi.org/10.1029/2012GL051319

Kohout, T., Havrila, K., Tóth, J., Husárik, M., Gritsevich, M., Britt, D., et al. (2014). Density, porosity and magnetic susceptibility of the Kosice meteorite shower and homogeneity of its parent meteoroid. *Meteoritics & Planetary Science*, *93-94*, 96–100. https://doi.org/10.1016/j.pss.2014.02.003

Kohout, T., Kiuru, R., Montonen, M., Scheirich, P., Britt, D., Macke, R., et al. (2011). Internal structure and physical properties of the Asteroid 2008 TC3 inferred from a study of the Almahata Sitta meteorites. *Icarus*, *212*(2), 697–700. https://doi.org/10.1016/j.icarus.2011.01.037

Kohout, T., Kletetschka, G., Elbra, T., Adachi, T., Mikula, V., Pesonen, L. J., et al. (2008). Physical properties of meteorites—Application in space missions to asteroids. *Meteoritics & Planetary Science*, *43*(6), 1009–1020. https://doi.org/10.1111/j.1945-5100.2008.tb00689.x

Kowitz, A., Güldemeister, N., Reimold, W. U., Schmitt, R. T., & Wünnemann, K. (2013). Diaplectic quartz glass and SiO_2 melt experimentally generated at only 5 GPa shock pressure in porous sandstone: Laboratory observations and meso-scale numerical modeling. *Earth and Planetary Science Letters*, *384*, 17–26. https://doi.org/10.1016/j.epsl.2013.09.021

Kukkonen, I. T., & Pesonen, L. J. (1983). Classification of meteorites by petrophysical methods. *Bulletin of the Geological Society of Finland*, *55*(2), 157–177. https://doi.org/10.17741/bgsf/55.2.005

Li, S. J., Wang, S. J., Leya, I., Li, Y., Li, X. Y., & Smith, T. (2017). Petrology, mineralogy, porosity, and cosmic-ray exposure history of Huaxi ordinary chondrite. *Meteoritics & Planetary Science*, *52*(5), 937–948. https://doi.org/10.1111/maps.12842

Li, S. J., Wang, S. J., Leya, I., Smith, T., Tang, J. L., Wang, P., et al. (2017). A chondrite strewn field was found in east of Lop Nor, Xinjiang (in Chinese). *Chinese Science Bulletin*, *62*(21), 2407–2415. https://doi.org/10.1360/N972016-01450

Li, S. J., Wang, S. J., Li, X. Y., Li, Y., Liu, S., & Coulson, I. M. (2012). A new method for the measurement of meteorite bulk volume via ideal gas pycnometry. *Journal of Geophysical Research*, *117*, E10001. https://doi.org/10.1029/2012JE004202

Macke, R. J. (2010). Survey of meteorite physical properties: Density, porosity and magnetic susceptibility Ph D. dissertation. University of Central Florida, Orlando.

Macke, R. J., Britt, D. T., & Consolmagno, G. J. (2010). Analysis of systematic error in bead method measurements of meteorite bulk volume and density. *Planetary and Space Science*, *58*(3), 421–426. https://doi.org/10.1016/j.pss.2009.11.006

Macke, R. J., Britt, D. T., & Consolmagno, G. J. (2011). Density, porosity, and magnetic susceptibility of achondritic meteorites. *Meteoritics & Planetary Science*, *46*(2), 311–326. https://doi.org/10.1111/j.1945-5100.2010.01155.x

Macke, R. J., Consolmagno, G. J., & Britt, D. T. (2011). Density, porosity, and magnetic susceptibility of carbonaceous chondrites. *Meteoritics & Planetary Science*, *46*(12), 1842–1862. https://doi.org/10.1111/j.1945-5100.2011.01298.x

Macke, R. J., Consolmagno, G. J., Britt, D. T., & Hutson, M. L. (2010). Enstatite chondrite density, magnetic susceptibility, and porosity. *Meteoritics & Planetary Science*, *45*(9), 1513–1526. https://doi.org/10.1111/j.1945-5100.2010.01129.x

Marchis, F., Descamps, P., Hestroffer, D., & Berthier, J. (2005). Discovery of the triple asteroidal system 87 Sylvia. *Nature*, *436*(7052), 822–824. https://doi.org/10.1038/nature04018

Matsui, T., Hamano, Y., & Honda, M. (1980). Porosity and compressional-wave velocity measurement of Antarctic meteorites. *National Institute of Polar Research*, *17*, 268–275.

McCausland, P. J. A., Brown, P. G., & Holdsworth, D. W. (2010). Rapid, reliable acquisition of meteorite volumes and internal features by laboratory X-ray micro-CT scanning, Lunar Planet. Sci. Conf., *41*, 1533.

McCausland, P. J. A., Samson, C., & Mcleod, T. (2011). Determination of bulk density for small meteorite fragments via visible light 3-D laser imaging. *Meteoritics & Planetary Science*, *46*(8), 1097–1109. https://doi.org/10.1111/j.1945-5100.2011.01217.x

Merrill, G. P., & Stokes, H. N. (1900). A new stony meteorite from Allegan, Michigan, and a new iron from Mart, Texas. *Journal of the Washington Academy of Sciences*, *2*, 41–68.

Ostro, S. J., Margot, J. L., Benner, L. A. M., Giorgini, J. D., Scheeres, D. J., Fahnestock, E. G., et al. (2006). Radar imaging of binary near-Earth asteroid (66391) 1999 KW4. *Science*, *314*(5803), 1276–1280. https://doi.org/10.1126/science.1133622

Pesonen, L. J., Terhoand, M., & Kinnumen, I. T. (1993). Physical properties of 368 meteorites: Implications for meteorite magnetism and planetary geophysics. *Proceedings of the NIPR Symposium on Antarctic Meteorites*, *6*, 401–416.

Petit, J.-M., Durda, D. D., Greenberg, R., Hurford, T. A., & Geissler, P. E. (1997). The long-term dynamics of Dactyl's orbit. *Icarus*, *130*(1), 177–197. https://doi.org/10.1006/icar.1997.5788

Pourkhorsandi, H., Gattacceca, J., Rochette, P., D'Orazio, M., Kamali, H., Avillez, R., et al. (2019). Meteorites from the Lut Desert (Iran). *Meteoritics & Planetary Science*, *54*(8), 1737–1763. https://doi.org/10.1111/maps.13311

Przylibski, T. A., Pilski, A. S., Zagozdzon, P. P., & Kryza, R. (2003). Petrology of the Baszkowka L5 chondrite: A record of surface-forming processes on the parent body. *Meteoritics & Planetary Science*, *38*(6), 927–937. https://doi.org/10.1111/j.1945-5100.2003.tb00288.x

Rabinowitz, D. L., Toutellotte, S., Brown, M. E., & Trujillo, C. (2005). Photometric observations of a very bright TNO with an extraordinary lightcurve (abstract). *Bulletin of the American Astronomical Society*, *37*, 746.

Sasso, M. R., Macke, R. J., Boesenberg, J. S., Britt, D. T., Rivers, M. L., Ebel, D. S, et al. (2009). Incompletely compacted equilibrated ordinary chondrites. *Meteoritics & Planetary Science*, *44*(11), 1743–1753. https://doi.org/10.1111/j.1945-5100.2009.tb01204.x

Schaefer, L., & Fegley, B. Jr. (2009). Volatile element chemistry during metamorphism of ordinary chondritic material and some of its implications for the composition of asteroids. *Icarus*, *205*(2), 483–496. https://doi.org/10.1016/j.icarus.2009.08.025

Scheeres, D. J., Ostro, S. J., Hudson, R. S., De Jong, E. M., & Suzuki, S. (1998). Dynamics of orbits close to Asteroid 4179 Toutatis. *Icarus*, *132*(1), 53–79. https://doi.org/10.1006/icar.1997.5870

Shen, W. J., Hu, S., Lin, Y. T., & Miao, B. K. (2013). Chemical and petrologic study of the Heyetang meteorite (in Chinese with English abstract). *Polar Research*, *25*(4), 386–393. https://doi.org/10.3724/SP.J.1084.2013.00386

Shepard, M. K., Richardson, J., Taylor, P. A., Rodriguez-Ford, L. A., Conrad, A., Peter, I., et al. (2017). Radar observations and shape model of asteroid 16 Psyche. *Icarus*, *281*, 388–403. https://doi.org/10.1016/j.icarus.2016.08.011

Smith, D. L., Samson, C., Herd, R., Deslauriers, A., Sink, J.-E., Christite, I., et al. (2006). Measuring the bulk density of meteorites non-destructively using three-dimensional laser imaging. *Journal of Geophysical Research*, *111*, E10002. https://doi.org/10.1029/2005JE002623

Stöffler, D. (1984). Glasses formed by hypervelocity impact. *Journal of Non-Crystalline Solids*, *67*, 465–502.

Stöffler, D., & Grieve, R. A. F. (2007). Impactites—A proposal on behalf of the IUGS sub-commission on the Systematics of metamorphic rocks. In D. Fettes, & J. Desmons (Eds.), *Metamorphic Rocks – A Classification and Glossary of Terms*. (pp. 82–92). Chapter 2.11. Cambridge: Cambridge University Press.

Stöffler, D., Keil, K., & Scott, E. R. D. (1991). Shock metamorphism of ordinary chondrites. *Geochimica et Cosmochimica Acta*, *55*(12), 3845–3867. https://doi.org/10.1016/0016-7037(91)90078-J

Strait, M. M., & Consolmagno, G. J. (2002). The nature and origin of meteorite porosity: Evidence from thin section analysis (abstract). *Meteoritics & Planetary Science*, *37*, A137.

Strait, M. M., & Consolmagno, G. J. (2005). Validation of methods used to determine microcrack porosity in meteorites. *Lunar and Planetary Science Conference*, *36*, 2073.

Terho, M., Pesonnen, L. J., & Kukkonen, I. T. (1993). The petrophysical classification of meteorites. *Studia Geophysica et Geodaetica*, *37*(1), 65–82.

Viateau, B., & Rapaport, M. (1997). The Bordeaux meridian observations of asteroids. First determination of the mass of (11) Parthenope. *Astronomy and Astrophysics*, *320*, 652–658.

Wang, D. D. (1993). *The introduction of China meteorite* (p. 62). Beijing: Science Press.

Wang, D. D., & Rubin, A. E. (1987). Petrology of nine ordinary chondrite falls from China. *Meteoritics*, *22*(1), 97–104. https://doi.org/10.1111/j.1945-5100.1987.tb00886.x

Wilkison, S. L., McCoy, T. J., McCamant, J. E., Robinson, M. S., & Britt, D. T. (2003). Porosity and density of ordinary chondrites: Clues to the formation of friable and porous ordinary chondrites. *Meteoritics & Planetary Science*, *38*(10), 1533–1546. https://doi.org/10.1111/j.1945-5100.2003.tb00256.x

Wilkison, S. L., & Robinson, M. S. (2000). Bulk density of ordinary chondrite meteorites and iplications for asteroidal internal structure. *Meteoritics & Planetary Science*, *35*(6), 1203–1213. https://doi.org/10.1111/j.1945-5100.2000.tb01509.x

Wittmann, A., Friedrich, J. M., Troiano, R. J., Macke, D. T., Britt, T. D., Swindle, J. R, et al. (2011). H/L chondrite LaPaz Icefield 031047—A feather of Icarus? *Geochimica et Cosmochimica Acta*, *75*(20), 6140–6159. https://doi.org/10.1016/j.gca.2011.07.037

Wood, J. A. (1967). Chondrites: their metallic minerals, thermal histories and parent planets. *Icarus*, *6*(1-2), 1–49. https://doi.org/10.1016/0019-1035(67)90002-4

Xie, X. D., Chen, M., & Wang, D. Q. (2001). Shock-related mineralogical features and P-T history of the Suizhou L6 chondrite. *European Journal of Mineralogy*, *13*(6), 1177–1190. https://doi.org/10.1127/0935-1221/2001/0013-1177

Xu, Y. C., Wang, S. J., Hu, S., Ouyang, Z. Y., & Lin, Y. T. (2016). Petrology, mineralogy and shock metamorphism of the Chelyabinsk meteorite (in Chinese with English abstract). *Acta Petrologica Sinica*, *32*(5), 1581–1590.

Yeomans, D. K., Antreasian, P. G., Barriot, J., Chesley, S. R., Dunham, D. W., Farquhar, R. W., et al. (2000). Radio science results during the NEAR-shoemaker spacecraft rendezvous with Eros. *Science*, *289*(5487), 2085–2088. https://doi.org/10.1126/science.289.5487.2085

Yomogida, K., & Matsui, T. (1981). Physical properties of some Antarctic meteorites. *National Institute Polar Research Memoirs*, *2*, 384–394.

Yomogida, K., & Matsui, T. (1983). Physical properties of ordinary chondrites. *Journal of Geophysical Research*, *88*(B11), 9513–9333. https://doi.org/10.1029/JB088iB11p09513